Received: 2 May 2022 | Accepted: 30 August 2022

DOI: 10.1002/vzj2.20233

Vadose Zone Journal

SPECIAL SECTION: EMERGING PARTICLES AND BIOCOLLOIDS IN TERRESTRIAL AND AQUATIC SYSTEMS

Colloidal transport of heavy metals in low-advective-velocity environmental systems: Reactive transport model on biogeochemical and hydrodynamic impacts

S. Sevinç Şengör | **Kahraman Ünlü**

Dep. of Environmental Engineering, Middle East Technical Univ., Dumlupınar Bulvarı No. 1, Ankara 06800, Turkey

Correspondence:
S. Sevinç Şengör, Dep. of Environmental Engineering, Middle East Technical Univ., Dumlupınar Bulvarı No. 1, 06800 Ankara, Turkey.
E-mail: ssengor@metu.edu.tr

Assigned to Associate Editor Constantinos Chrysikopoulos.

Funding information
2236 Co-Funded Brain Circulation Scheme2 (CoCirculation2) of TÜBİTAK, Grant/Award Number: 120C053

Abstract

In this study, the impact of colloid facilitated transport of heavy metals on the overall biogeochemical processes is demonstrated in example Lake Coeurd'Alene sediments. Release and transport of heavy metals (Pb and Zn) on initially sorbed colloidal Fe (hydr)oxide minerals are compared with immobile surfaces under various advective flow velocities. The reactive transport model integrates a coupled biotic reaction network with multiple terminal electron acceptors, including multicomponent diffusion and electrostatic double layer (EDL) treatment effects, illustrating the impact of colloidal transport under competing biogeochemical reaction dynamics for the first time to the authors' knowledge. The model results illustrate the sensitivity of the results under low-flow-velocity conditions. Although enhanced Fe reduction prevails with immobile Fe (hydr)oxide mineral surfaces, the desorbed metal ions with aqueous sulfide complexes are rather "washed out" from the system along with advective transport of solutes, whereas the reductive dissolution of colloidal Fe (hydr)oxides from freshly coming colloidal surfaces results in the accumulation of metal and sulfide ions in the system. The results show that when the potential transport of sorbed contaminants with colloidal particles are ignored, the contaminant concentrations might be underestimated under low-flow-velocity conditions, especially around 10^{-8} or 10^{-9} m s^{-1}, where the underestimation for the worst case scenario at the lowest bound of low-flow-velocity conditions may reach around 90% with depth. On the other hand, this impact may be less significant under cases of higher flow velocity, even around higher limits of low-velocity environments around 10^{-7} m s^{-1}, as well as in pure diffusive transport cases.

Abbreviations: EDL, electrostatic double layer; FRB, iron-reducing bacteria; HFO, hydrous ferric oxide; LCdA, Lake Coeurd'Alene; SRB, sulfate-reducing bacteria.

1 | Introduction

Colloids are nanoscopic particles with diameter in the range of 1 nm to 10 μm and are widely distributed in the environment (Bin et al., 2011; Montalvo & Smolders, 2019). These colloids have recently been gaining significant attention due to their unique characteristics in environmental remediation pertaining to degradation, transformation, and immobilization of contaminants in soils and aquifers. However, once mobilized by subsurface water flow, colloids may pose risks to surface water and groundwater quality as they are effective ''carriers'' of a variety of common contaminants found in soils and water (Amde et al., 2017). Due to their high specific surface areas, high reactive site densities, and high mobility in soils, the colloids facilitate the sorption and thus the transport of many contaminants in the subsurface, such as heavy metals, radionuclides, and organic compounds, which are otherwise immobile with limited solubility in the aqueous environment (Kretzschmar et al., 1999; Ryan & Elimelech, 1996; Thompson et al., 2006). Various researchers have studied the mobility of contaminants via colloidal particles, showing the facilitation of pollution transport in the subsurface systems (e.g., Benhabib et al., 2017; Cheng et al., 2016; de Jonge et al., 2004; Emerson et al., 2016; Ma et al., 2017; Sen et al., 2002a, 2002b; Šimůnek et al., 2006; Snousy et al., 2018; Zhuang et al., 2003), whereas others have demonstrated the adsorbed contaminants to be trapped among sediment grains, impeding pollution transport (e.g., Bekhit et al., 2006, 2009; Ghiasi et al., 2020b; Kheirabadi et al., 2017; Peng et al., 2017; Sen & Khilar, 2006). Katzourakis and Chrysikopoulos (2015) developed a three-dimensional numerical model to investigate the simultaneous transport (co-transport) of dense colloids and viruses in porous media. Their work showed that the presence of dense colloidal particles can either enhance or hinder the horizontal transport of viruses, but can also increase the vertical migration of viruses in homogeneous and saturated porous media.

The mobilization of colloid particles strongly depends on solution pH, ionic strength, and ionic composition of the aqueous solution, as the abovementioned parameters affect the surface charge of the colloidal particle (Stumm, 1977; Thompson et al., 2006). The adsorption or surface complexation of metal oxide colloidal particles strongly depends on their surface charge, which results in an electrostatic double layer (EDL) that forms around the oxide surface (Bourikas et al., 2001; Fatehah et al., 2014). Two liquid layers around the oxide particle form. In the inner layer (also called Stern layer), ions are strongly bound to the surface, whereas in the diffuse layer, counter ions are surrounded (with different potentials corresponding to Debye length), and it moves along with the moving colloidal particle, impacting the overall distribution of ions in the surrounding medium (Fatehah et al., 2014). Transport behavior of ions and tracers in bentonite and clay systems, including implementations of EDL models, has been studied previously (e.g., Alt-Epping et al., 2015; Appelo et al., 2008, 2010; Appelo & Wersin 2007; Tournassat & Appelo, 2011). The impact of solution composition—particularly pH, ionic strength, flow velocity, colloidal particle concentration, and size—has been demonstrated extensively by various researchers (Borgnino 2013; Bradford et al., 2002; He et al., 2019; X. Li et al., 2019; Roy & Dzombak, 1997; Ryan & Elimelech, 1996; Torkzaban et al., 2015; Um & Papelis, 2002). The coupled effects of ionic strength, particle size, and flow velocity on transport and deposition of suspended particles were investigated by Bennacer et al. (2017), proposing a relationship among the deposition kinetics, particle and grain sizes, flow velocity, and ionic strength. Ghiasi et al. (2020a) studied the impact of colloid concentration, flow velocity, and sand gradation on co-transport of Cr(VI) and bentonite colloids.

The colloids are mainly derived particulates from clay minerals, Fe oxides, Al, silicate, and natural organic substances (Ghiasi et al., 2020a; Sen & Khilar, 2006). Iron (hydr)oxide nanoparticles often form in natural waters and at oxic–anoxic boundaries in sediments, and it is well established that they can control the solid–solution partitioning of numerous toxic metal species in near-surface aqueous regimes (Amde et al., 2017). Thus, Fe (hydr)oxide compounds and their colloidal counterparts have significant applications in soil and groundwater remediation due to their large surface areas, self-assembly potential, high specificity, and high reactivity characteristics, which can lead to spontaneous adsorption and co-precipitation of heavy metals. Moreover, nanoparticle materials have the potential to be effectively transported by groundwater and may be easily injected as subcolloidal oxides, hydroxides, and/or oxyhydroxides into contaminated soils, sediments, and aquifers due to their large susceptibility to form and exist in suspension in an aqueous medium (Litter et al., 2018). In addition to the abiotic factors, the Fe redox cycle and microbial Fe reduction affect the solution chemistry through biogeochemical pathways, as well as promoting colloid dispersion (Thompson et al., 2006). The impact of

Core Ideas

- Colloidal transport of Fe (hydr)oxide particles with complex biogeochemical dynamics is presented.
- Enhanced control of Fe reduction by Fe-reducing bacteria with immobile Fe (hydr)oxide mineral surfaces is observed.
- Sensitivity of the colloidal transport of contaminants under low-flow-velocity conditions is observed.
- Absence of colloidal particle transport might underestimate transport of sorbed contaminants.

Fe redox cycles on colloid-bound natural organic matter and metals in a soil system is investigated by Thompson et al. (2006). The hydrological and hydrochemical parameter (ionic strength and flow rate) effect on the control and mobility of ferrihydrite colloids in sand columns is studied by Tosco et al. (2012); where a correlation to estimate the travel distance of ferrihydrite nanoparticles in field environments is proposed.

Although various studies have investigated colloid mobility and transport, including the impacts of various environmental conditions and parameters such as pH, ionic strength, flow velocity, and colloid aggregate size and concentration on pollutant transport (especially under well-controlled laboratory experiments), the impact of colloidal transport on heavy metal release under complex biogeochemical dynamics in natural subsurface settings has been highly limited. The biogeochemical redox dynamics exert significant controls on heavy metal distribution within the mobile and immobile (mineral) phases, especially considering the delicate interplay of Fe and S species and associated minerals on redox sensitive metals. Microbially mediated reductive dissolution of (hydr)oxides generally decreases the effective surface area of the mineral, resulting in the release of trace metals and potentially the precipitation of secondary phases (Amde et al., 2017; Wang et al., 2012). It is important to incorporate these interactive and critical processes into colloidal fate and reactive transport models to better understand the implications for mobilization of sorbed contaminants and heavy metal species in subsurface environments. Therefore, the goal of this study is to investigate the impact of colloidal Fe (hydr)oxide particles on the transport of heavy metal species (Zn and Pb) in a *natural subsurface* environment, integrating coupled microbially mediated consortium biodegradation kinetics with abiotic reaction network dynamics. The particular focus is to investigate the impact of initially sorbed heavy metal dynamics under the integrated biogeochemical conditions with a complete (unhindered) colloidal transport of Fe (hydr)oxide phases through comparisons with immobile counter-phases. Although the work presented here demonstrates these processes in an example lake sediment system, the results can be extended to other low-advective-velocity subsurface systems such as flow through low-permeability clay lenses in heterogeneous aquifers, leakage through aquitards overlaying confined aquifers, leakage through compacted clay liners, underground storage tanks, vertical cutoff walls, and surface impoundments.

2 | Colloidal reactive transport model

2.1 | Modeling approach

In this study, the impact of colloid-facilitated transport of Fe (hydr)oxide minerals on the mobility of heavy metals (Pb, Zn) under biogeochemical dynamics is presented using previous work of Şengör, Spycher, Ginn, Moberly, et al. (2007) and Şengör, Spycher, Ginn, Sani, et al. (2007) and J. Li and Şengör (2020) on Lake Coeurd'Alene (LCdA) sediments as an example. Şengör, Spycher, Ginn, Moberly, et al. (2007) and Şengör, Spycher, Ginn, Sani, et al. (2007) developed a one-dimensional reactive transport model to evaluate the fate and mobility of heavy metals (i.e., Zn, Pb, and Cu) in LCdA sediments, initially sorbed onto Fe (hydr)oxide mineral phases. The solubilization (and hence mobilization) of metals as a result of microbial reductive dissolution of Fe (hydr)oxide minerals by Fe-reducing bacteria (FRB) vs. metal precipitation at sediment depth as metal sulfide precipitates as a result of microbially mediated formation of sulfide by sulfate-reducing bacteria (SRB) has been modeled, and these competing processes were investigated. The model results revealed the relative rates of FRB and SRB to exert significant control over the solution biochemistry and pH within the sediment depth, which influenced the dynamics of heavy metals in the system. The details of the solid phase and pore water chemistry, sediment, and water sample data that were compiled from other studies on LCdA system are provided in Şengör, Spycher, Ginn, Sani, et al. (2007). J. Li and Şengör (2020) presented a continuation of the work by Şengör, Spycher, Ginn, Moberly, et al. (2007) and Şengör, Spycher, Ginn, Sani, et al. (2007) illustrating the competitive effects of FRB and SRB activities on pH and overall biogeochemical dynamics including multispecies diffusion and explicit treatment of electrostatic effects in the LCdA system. Their results showed the significance of multicomponent diffusion (as opposed to the use of single uniform diffusion coefficient for all species) and EDL effects in purely diffusion-dominated sediments on predicting the mobility of heavy metals under complex biogeochemical conditions.

The reactive transport models previously studied by Şengör, Spycher, Ginn, Moberly, et al. (2007) and Şengör, Spycher, Ginn, Sani, et al. (2007) and J. Li and Şengör (2020) were based on immobile Fe (hydr)oxide mineral phases with sediment surface area and other characterizations of ferrihydrite mineral used from Şengör, Spycher, Ginn, Sani, et al. (2007). In this study, the impact of colloidal Fe (hydr)oxide mineral phases on the overall solution biogeochemistry and transport of ions is investigated using the previous biogeochemical model with the identical Fe (hydr)oxide mineral phase characteristics, but only considering these phases as fully mobile colloids under low-flow-velocity conditions. The model simulation results are compared with previous immobile Fe (hydr)oxide phases, demonstrating the role of colloidal-facilitated transport of ions under complex biogeochemical processes within a realistic subsurface system setting, using LCdA just as an example. It should be noted that as the mere goal of this study is to investigate the (unhindered) colloidal transport of Fe (hydr)oxide phases by comparing

them with immobile mineral counter-phase responses to the overall system dynamics, the colloid deposition, attachment, and/or straining characteristics are not considered here, with the intention of avoiding any retaining or hindering influences of colloidal transport. In the model presented here, colloids are advectively transported at the same velocity as the solutes (metal ions) in the vertical column. In other words, colloids are suspended and fully mobile in the pore water during advective transport under low-flow-velocity conditions without any tendency of attachment or deposition onto aquifer matrix. The suspension and mobility of colloidal particles in the pore water are enhanced by the repulsive interactions present between strongly and similarly charged colloids and the aquifer matrix. Therefore, this argument can be realistic in most porous systems where nano-sized particle transport is occurring. The results allow the assessment of kinetic effects of competing coupled biotic and abiotic reaction dynamics with unhindered transport of colloidal Fe (hydr)oxide phases under low-flow-velocity environments that can typically be encountered in a natural subsurface setting.

2.2 | Key parameters of transport processes

The simulation results presented in this study are carried out with the reactive transport code PHREEQC (Parkhurst & Appelo, 2013). The parameters of transport processes considered in this work include advective transport and multispecies diffusion (species-specific multicomponent diffusion), and colloidal Fe (hydr)oxide phase transport with EDL treatment of ferrihydrite surfaces. Hydrodynamic dispersion is ignored. These processes are described briefly below.

The governing equation for mass transport in the macroporosity domain is as follows (Alt-Epping et al., 2015; Steefel, Mayer, et al., 2015):

$$\frac{\partial\left(\phi^{B}C_j\right)}{\partial t}=\nabla\cdot\left(\phi^{B}D_j^{*}\nabla\right)-\nabla\cdot\left(qC_j\right)-\sum\nolimits_{n=1}^{N_n}\upsilon_{jn}R_n \tag{1}$$

where C_j is the concentration of the jth primary species in solution; ϕ^{B} is the macroporosity; q is the Darcy flux, and D_j^{*} is the molecular pore diffusion coefficient of the jth species. The reaction term includes N_n kinetically controlled mineral reactions with the corresponding stoichiometric coefficients (υ_{jn}) and rates (R_n). It should be noted that gravity is implicitly considered during solute transport in Equation 1, where Darcy flux q, in turn advective vertical flow velocity v, accounts for the effect of gravity on solute transport, because the sediment system is modeled as a one-dimensional vertical column under steady-state flow (constant total hydraulic head gradient, being the sum of the pressure and gravitational head components) conditions. It is assumed that colloids are advectively transported at the same velocity as the solutes (metal ions) in the vertical column. In addition, because the colloids are suspended in the pore water and electrostatically not attracted to aquifer matrix during advective transport, they are not subjected to additional significant gravitational settlement forces. Considering the electrostatic forces induced by species of nonzero charge, the implementation of multispecies diffusion considered in the study includes the involvement of electrochemical potential for the transport of ions in the solution, where positively and negatively charged species maintain local charge balance. Therefore, the diffusion of species j depends on the concentration gradient of itself, as well as other charged species in the solution represented as (e.g. Bard & Faulkner, 2001; Steefel & Maher, 2009; Steefel, Yabusaki, & Mayer, 2015):

$$J_j=-\phi D_j^{*}\nabla C_j-\frac{\phi D_j^{*}C_j}{RT}z_jF\nabla\Psi \tag{2}$$

where J is the diffusive flux, Ψ is the electrochemical potential, z_j is the charge of jth species, F and R are the Faraday and gas constants, respectively, and T is the absolute temperature.

In PHREEQC, the changes in solution composition due to advection, dispersion, and/or diffusion are coupled with reversible and irreversible chemical reactions within the column. For simulating colloidal transport, colloids are given a diffusion coefficient and transported as solutes through the column (Parkhurst & Appelo, 2013).

The EDL effects are implemented involving the species-specific diffusion coefficients of ions in pore water and an EDL that compensates the surface charge of Fe hydroxide (i.e., ferrihydrite). PHREEQC is one of the few continuum-based reactive transport codes that can simulate the solution chemistry and species transport with an explicit treatment of an EDL. In PHREEQC implementation of EDL, the total pore space in the system is considered to be composed of two porosity domains: the microporosity domain (interlayer space and the EDL) and the macroporosity domain that consists of charge balanced water (Alt-Epping et al., 2015). The governing equation for the EDL porosity is expressed by (Alt-Epping et al., 2015):

$$\frac{\partial\left(\phi^{EDL}C_j^{EDL}\right)}{\partial t}=\nabla\cdot\left(\phi^{EDL}D_j^{EDL}C_j^{EDL}\right) \tag{3}$$

where ϕ^{EDL} is the EDL porosity, C_j^{EDL} is the total concentration in the EDL, and D_j^{EDL} is the species-specific diffusion coefficient in the ED. All precipitation and dissolution reactions are assumed to take place in the macroporosity domain, and only the water within the macroporosity domain moves in response to a gradient. Transport within the EDL domain is considered to be purely diffusive. In PHREEQC,

the electrical potential and species distribution in the EDL are described by a Donnan approach, which assumes a single electrical potential in the EDL and an instantaneous equilibrium of species between the EDL and the free water (i.e., between the microporosity and macroporosity domains). The details of the Donnan approximation and its implementation in PHREEQC is discussed in detail by Parkhurst and Appelo (2013), Alt-Epping et al. (2015), and J. Li and Şengör (2020).

For the system simulated in this study, based on the ionic strength of the pore-water composition (0.0035 M), the Debye length of the EDL can be calculated using the formulations presented in Alt-Epping et al. (2015) and J. Li and Şengör (2020) as 4.98×10^{-8} m, which corresponds to 50% of microporosity volume. Considering the EDL Debye length calculations reported in the literature (e.g., Holmboe et al., 2012; Parkhurst & Appelo, 2013; Tournassat & Appelo, 2011), this volume percentage is within the reported values, and therefore the simulations have been carried out using 50% microporosity. Although simulation results were not significantly sensitive to the microporosity volume (%) considered for the EDL Debye length, the results were observed to be significantly affected by EDL consideration, compared with no EDL implementation in the system. Therefore, all simulations have been run with EDL considerations. In fact, when modeling colloidal surfaces, the Donnan approach balances the accumulation of surface charge with an explicit calculation of the diffuse layer composition. Therefore, its use is essential, especially to assure electrically neutral solution when the surfaces are separated from the solution (Parkhurst & Appelo, 2013).

The relationship between effective diffusion coefficient D_j^e, pore diffusion coefficient D_j^*, and diffusion coefficient in "free" water D_j^0 is provided below (Alonso et al., 2007). The diffusion coefficient of a spherical particle in an unconfined liquid (D_j^0) can be calculated using the Stokes–Einstein equation as (e.g. Alonso et al., 2007):

$$D_j^0 = \frac{kT}{6\pi\eta r} \tag{4}$$

where k is the Boltzmann constant, T is temperature, η is the dynamic viscosity of the liquid (water), and r is the hydrodynamic radius of the particle. The pore water diffusion coefficient D_j^* is expressed as

$$D_j^* = D_j^0 \frac{\delta}{\tau^2} \tag{5}$$

$$D_j^e = \varepsilon D_j^* \tag{6}$$

where τ is tortuosity and δ is constrictivity that hinders diffusion in solids (Alonso et al., 2007; Buil, 2002). ε is the accessible porosity in the porous medium. The ratio $\frac{\delta}{\tau^2} = G$ is geometric factor, which is less than 1 (Alonso et al., 2007). An empirical relationship between G and ε in crystalline rocks is $G = 0.71\varepsilon^{0.58}$ (Jakob, 2004; Parkhomenko, 1967).

TABLE 1 The diffusion coefficient in "free" water (D_j^0), pore diffusion coefficient (D_j^*), and effective diffusion coefficient (D_j^e) values for the hydrous ferric oxide colloidal particles used in this study

Parameter	Value
Colloidal particle radius, m	1.27×10^{-8}
D_j^0, m^2 s^{-1}	1.93×10^{-11}
D_j^*, m^2 s^{-1}	3.11×10^{-12}
D_j^e, m^2 s^{-1}	2.42×10^{-13}

In this study, the colloidal particle radius is calculated using the specific surface area (SSA) of ferrihydrite (205 m^2 g^{-1}, as discussed previously by Şengör, Spycher, Ginn, Sani, et al. [2007]). For a particle of spherical shape, the relationship between SSA and particle radius (r) is given as (Séquaris et al., 2013):

$$\text{SSA} = \frac{4r^3}{4/3r^3\sigma} = \frac{3}{r\sigma} \tag{7}$$

where σ is the particle density, which is 1.15 g cm^{-3} for ferrihydrite particles (Şengör, Spycher, Ginn, Sani, et al., 2007). From Equation 7, the radius of particles is calculated to be 1.27×10^{-8} m or 12.73 nm.

Considering the dynamic viscosity of water to be $\eta = 8.9 \times 10^{-4}$ Pa s^{-1}, Boltzmann constant (k) = $1.38064852 \times 10^{-23}$ m^2 kg s^{-2} K^{-1}, and T = 298 K, the D_j^0 value for the ferrihydrite colloidal particles in this study is calculated to be 1.93×10^{-11} m^2 s^{-1} using Equation 4. As mentioned in previous discussions for LCdA sediments (J. Li and Şengör, 2020), the average porosity for the sediments was 0.776. After the discussions in Alonso et al. (2007), the accessible porosity is taken to be one order of magnitude lower than the average porosity (0.0776), due to the anionic exclusion of colloids during colloidal transport (considering the negative charge on both colloids and porous medium) (Alonso et al. 2007; Ohlsonn & Neretnieks, 1997). Therefore the D_j^* and D_j^e values for the colloidal ferrihydrite particles in this study are calculated from Equations 5 and 6 as 3.11×10^{-12} and 2.42×10^{-13} m^2 s^{-1}, respectively (Table 1). Alonso et al. (2007) obtained D_j^* values ranging from 5.83×10^{-13} to 3.32×10^{-14} m^2 s^{-1} for 2.7-to-47.5-nm sized gold colloid particles.

Ferrihydrite aggregates are not regarded as a solid with a simple surface structure and geometry; therefore, diffusion coefficient measurements of ferrihydrite are not directly available (Braunschweig et al., 2014). Hofmann et al. (2004) estimated the diameter of hydrous ferric oxides crystallites by transmission electron microscopy to be 1.9 ± 0.5 nm.

Model simulations of higher and lower (around one order of magnitude) effective diffusion coefficients are also tested (results not shown) considering variations in hydrodynamic radius of ferrihydrite colloidal particles. The results did not show significant difference, and therefore an effective diffusion coefficient of 2.42×10^{-13} m^2 s^{-1} is being used throughout the simulations presented.

Four different flow velocities representative of subsurface systems that can be typically encountered, for example, in compacted clay liners widely used as hydraulic barriers in waste disposal systems (e.g., Javadi et al., 2017) are used to test the impact of hydrodynamic conditions on colloidal transport in this study: adv1 (9×10^{-9} m s^{-1}), adv2 (3×10^{-8} m s^{-1}), adv3 (9×10^{-7} m s^{-1}), and adv4 (3×10^{-7} m s^{-1}), which are within the range of values reported in the literature in similar porous systems. As the Peclet number indicates the dominance of advective vs. diffusive transport and because the LCdA system is diffusion dominated, appropriate Péclet number ranges are chosen accordingly. Considering solute molecular diffusion coefficient as 5.71×10^{-10} m^2 s^{-1}, tortuosity factor as 0.5, and average grain diameter as 3.5×10^{-5} m for the LCdA sediment system based on previous sediment analysis (Şengör, Spycher, Ginn, Sani, et al., 2007), advective velocity ranges are calculated corresponding to Péclet number ranges between 0.02 and 0.0006. Based on these ranges, four different velocities are considered accordingly: adv1 (9×10^{-9} m s^{-1} corresponding to Pe = 0.0006), adv2 (3×10^{-8} m s^{-1} corresponding to Pe = 0.002), adv3 (9×10^{-7} m s^{-1} corresponding to Pe = 0.06), and adv4 (3×10^{-7} m s^{-1} corresponding to Pe = 0.02), which are again within the range reported in the literature for similar porous systems (e.g., Javadi et al., 2017).

2.3 | Key input parameters of biotic and abiotic reaction systems

The input parameters of the inorganic and microbially mediated reaction network are based on previous works for the LCdA system (Şengör, Spycher, Ginn, Moberly et al., 2007; Şengör, Spycher, Ginn, Sani, et al., 2007; J. Li and Şengör 2020). The chemical and microbial reaction networks are also based on Şengör, Spycher, Ginn, Sani, et al. (2007) and are shown in Tables 2–5.

For the inorganic reaction system, the minerals included in the simulations are ferrihydrite [considered as colloidal $Fe(OH)_3$] and siderite ($FeCO_3$), which are initially present; and mackinawite (FeS_m, disordered), sphalerite (ZnS), and galena (PbS), which are initially absent and considered as secondary minerals. Table 2 details the geochemical reaction network and corresponding kinetic rate law expressions used in the model (Şengör, Spycher, Ginn, Sani, et al., 2007).

In the microbially mediated reaction system, the inorganic diffusive transport model is coupled to a biotic reaction network including biodegradation kinetics with multiple terminal electron acceptors and biotransformation dynamics of redox front. The microbially mediated reaction network and corresponding kinetic expressions are given in Table 3. The initial concentrations used in the model are provided in Table 4. Parameter values for the kinetic rate constants used in the biogeochemical model are listed in Table 5. The aqueous complexation reactions along with log K constants are provided in Supplemental Table S1.

3 | Results and discussion

The present study aims to investigate the impact of colloid facilitated transport of contaminants (heavy metals: Pb and Zn) on the overall dynamics of biogeochemical cycling of heavy metals in a natural subsurface environment. Using the LCdA system as an example field study, colloidal Fe hydroxide phases in the benthic sediment environment are modeled as mobile colloidal hydrous ferric oxide (HFO) particles with an effective diffusion coefficient of 2.42×10^{-13} m^2 s^{-1}. The colloidal Fe phases are modeled as being injected at the upper boundary, which are then transported along with other solutes along the depth of the sediment. A conceptual model illustrating the main processes implemented in the colloid-facilitated reactive transport model in this study is given in Figure 1. As seen from the illustrations in Figure 1, ferrihydrite colloids are considered as the major sorbing phase for heavy metals (Pb and Zn), where the metal adsorption is implemented by surface complexation using double layer modeling (Dzombak & Morel, 1990). Once the colloidal Fe phases enter the system at the upper boundary, heavy metals that simultaneously enter the column based on the (oxic) shorewater composition at the top boundary (Table 4) undergo instantaneous surface complexation reactions at equilibrium ($t = 0$ d). Heavy metals initially sorbed onto the colloidal Fe (hydr)oxide minerals are then mobilized through microbial reductive dissolution of FRB, resulting in Fe(II) ions and release of heavy metals into the solution. Sulfate reduction by SRB results in biogenic sulfide (HS^-) formation, which then becomes available to precipitate with free heavy metal ions [Zn, Pb, Fe(II)] in the porewater solution. Thus the precipitation of metal sulfides (ZnS, PbS, FeS) at depth as a result of biogenic sulfide production, as well as siderite ($FeCO_3$) precipitation, is captured in the model (Figure 1). The simulations have also been extended to investigate the impact of colloidal reactive transport on coupled biogeochemical reactions by testing increased and decreased rates of microbial Fe- and sulfate reduction. These particular considerations are described in detail below.

TABLE 2 Precipitation/dissolution reactions (from Şengör, Spycher, Ginn, Sani, et al., 2007; Li & Şengör 2020)

Mineral	Precipitation/dissolution reactions:	Kinetic rate (R) law expression
Ferrihydrite	$Fe(OH)_3 + 3H^+ \leftrightarrow Fe^{+3} + 3H_2O$	Equillibrium
Mackinawite	$FeS + H^+ \leftrightarrow Fe^{+2} + HS^-$	Equillibrium
Siderite	$FeCO_3 \leftrightarrow Fe^{+2} + CO_3^{-2}$	$R_{FeCO3} = 1 \times 10^{-12} \frac{SI_{FeCO3}}{\lvert SI_{FeCO3}\rvert + 0.5}$
Sphalerite	$ZnS + H^+ \leftrightarrow Zn^{+2} + HS^-$	$R_{ZnS} = 1 \times 10^{6}[Zn^{+2}][H_2S] \frac{SI_{ZnS}}{\lvert SI_{ZnS}\rvert + 0.5}$
Galena	$PbS + H^+ \leftrightarrow Pb^{+2} + HS^-$	$R_{PbS} = 1 \times 10^{6}[Pb^{+2}][H_2S] \frac{SI_{PbS}}{\lvert SI_{PbS}\rvert + 0.5}$
Chalcocite	$Cu_2S + H^+ \leftrightarrow 2Cu^+ + HS^-$	$R_{Cu2S} = 1 \times 10^{14}[Cu^+]^2[H_2S] \frac{SI_{Cu2S}}{\lvert SI_{Cu2S}\rvert + 0.5}$

TABLE 3 Microbially-mediated reactions and corresponding kinetic rate (R) expressions for the model system (from Şengör, Spycher, Ginn, Sani, et al., 2007; Li & Şengör 2020)

Expression type	Expression
Microbially mediated reactions	$CH_3COO^- + 2O_2 \leftrightarrow 2CO_3^{-2} + 3H^+ R_{O2}$
	$CH_3COO^- + 4NO_3^- \leftrightarrow 2CO_3^{-2} + 4NO_2^- + 3H^+ R_{NO3}$
	$CH_3COO^- + 8Fe^{+3} + 4H_2O \leftrightarrow 8Fe^{+2} + 2CO_3^{-2} + 11H^+ R_{Fe+3}$
	$CH_3COO^- + SO_4^{-2} \leftrightarrow 2CO_3^{-2} + HS^- + 2H^+ R_{SO4-2}$
Kinetic rate laws	$R_{O2} = V_m^{O2} \frac{[O_2]}{[O_2]+K_s^{O2}} \frac{\log(Q_{O2}/K_{O2})}{\log(Q_{O2}/K_{O2})+0.5_s}$
	$R_{NO3} = V_m^{NO3} \frac{[NO_3^-]}{[NO_3^-]+K_s^{NO3}} \frac{K_{O2}^{in}}{K_{O2}^{in}+[O_2]} \frac{\log(Q_{NO3}/K_{NO3})}{\log(Q_{NO3}/K_{NO3})+0.5}$
	$R_{Fe+3} = V_m^{Fe} \frac{K_{O2}^{in}}{K_{O2}^{in}+[O_2]} \frac{K_{NO3}^{in}}{K_{NO3}^{in}+[NO_3]} \frac{\log(Q_{Fe+3}/K_{Fe+3})}{\log(Q_{Fe+3}/K_{Fe+3})+0.5}$
	$R_{SO4-2} = V_m^{SO4} \frac{[SO_4^{-2}]}{[SO_4^{-2}]+K_s^{SO4}} \frac{K_{O2}^{in}}{K_{O2}^{in}+[O_2]} \frac{K_{NO3}^{in}}{K_{NO3}^{in}+[NO_3]} \times \frac{K_{Fe}^{in}}{K_{Fe}^{in}+[Fe^{+3}]} \frac{\log(Q_{SO4}/K_{SO4})}{\log(Q_{SO4}/K_{SO4})+0.5}$

Note. V_m^i, maximum substrate use rate constant using the ith terminal electron acceptor (TEA); K_s^i, half saturation constant for the ith TEA; K_i^{in}, inhibition constants due the ith TEA; Q_i, K_i, activity product and equilibrium constant for the corresponding TEA use reaction

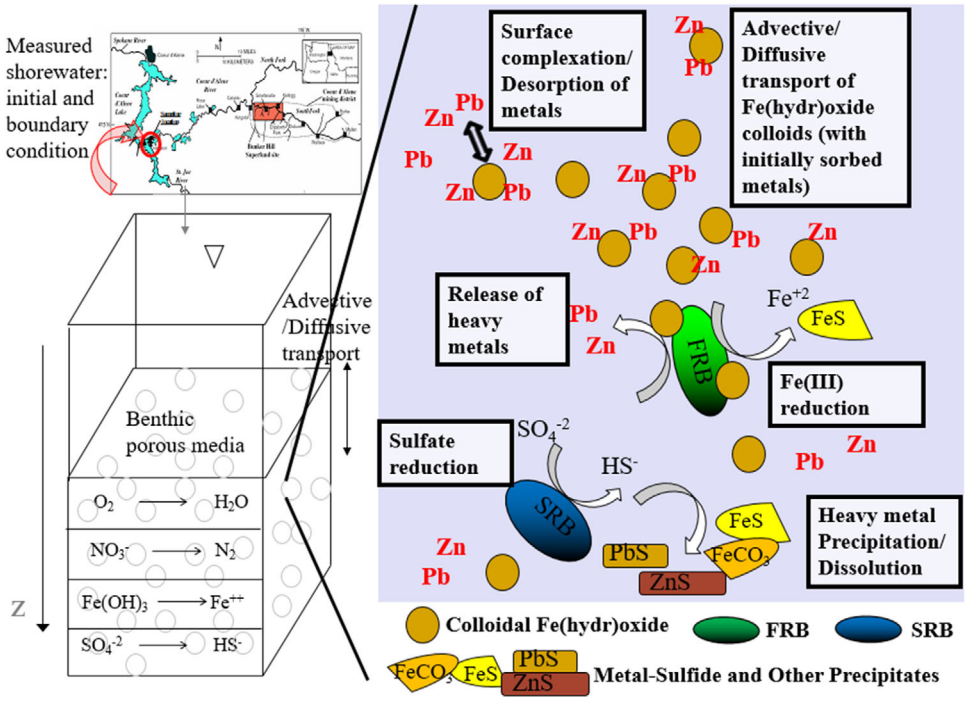

FIGURE 1 Conceptual model illustrating the processes implemented in the colloid-facilitated reactive transport model. FRB, Fe-reducing bacteria; SRB, sulfate-reducing bacteria

TABLE 4 Initial concentrations used in the model based on the (oxic) lake water composition at the top boundary (from Şengör, Spycher, Ginn, Sani, et al., 2007; Li & Şengör, 2020)

Aqueous species	Units	Value
pH		7.2
Total inorganic C	M	3.535×10^{-4}
Ca^{2+}	M	1.372×10^{-4}
Mg^{2+}	M	8.641×10^{-5}
Fe^{2+}	M	2.034×10^{-19} (≈ 0)
Fe^{3+}	M	3.009×10^{-9}
K^{+}	M	1.279×10^{-5}
S^{2-}	M	1.3093×10^{-142} (≈ 0)
SO_4^{-2}	M	5.830×10^{-5}
Na^{+}	M	1.000×10^{-4}
Cl^{-}	M	1.946×10^{-5}
$O_{2(aq)}$	M	2.700×10^{-4}[a]
NO_3^{-}	M	1.800×10^{-5}[a]
$N_{2(aq)}$	M	9.150×10^{-19} (≈ 0)
Pb^{2+}	M	5.309×10^{-8}
Cu^{+}	M	1.180×10^{-8}
Zn^{2+}	M	8.717×10^{-6}
Acetate^{-}	M	7.000×10^{-3}
Br^{-}	M	1.00×10^{-30} (≈ 0)

[a]Based on the saturation of O_2 under 25 °C and nitrate data from Winowiecki (2002).

TABLE 5 Parameter values for the kinetic constants used in the biogeochemical model (from Şengör, Spycher, Ginn, Sani, et al., 2007; Li & Şengör, 2020)

Parameter	Units	Value used in the model
V_m^{O2}	s^{-1}	5×10^{-9}[a]
V_m^{NO3-}	s^{-1}	2×10^{-10}[b]
V_m^{Fe3+}	s^{-1}	3×10^{-12}[c]
V_m^{SO42-}	s^{-1}	3×10^{-9}[c]
K_s^{O2}	M	2.41×10^{-5}[d]
K_s^{NO3-}	M	1.13×10^{-4}[d]
K_s^{SO42-}	M	1×10^{-3}[e]
K_{O2}^{in}	M	1.61×10^{-8}[d]
K_{NO3-}^{in}	M	1×10^{-7}[c]
K_{Fe3+}^{in}	M	1×10^{-8}[c]

Note. V_m^i, maximum substrate use rate constant using the ith terminal electron acceptor (TEA); K_s^i, half saturation constant for the ith TEA; K_i^{in}, inhibition constants due the ith TEA.

[a]Estimated from Russell (1973).

[b]Estimated from Parkhurst and Appelo (2013).

[c]Şengör et al. (2007b).

[d]Estimated from Doussan et al. (1997).

[e]Estimated from Brugato (1999).

The simulations have been conducted using four different flow velocities representative of low velocity subsurface systems that can be typically encountered in natural subsurface environments (e.g., Javadi et al., 2017): adv1 (9×10^{-9} m s^{-1}), adv2 (3×10^{-8} m s^{-1}), adv3 (9×10^{-7} m s^{-1}), and adv4 (3×10^{-7} m s^{-1}). Simulations with advective transport are also compared with pure diffusive transport runs. The model results are presented as computed concentrations as a function of sediment depth (40 cm) corresponding to 5 yr of simulated time periods, which is considered to be representative of steady-state conditions. The 40-cm sediment depth in the model results is chosen based on a representative depth that is adequate to capture the main trends of key species during the transitioning from suboxic to anoxic conditions, as well as the redox disequilibrium conditions occurring within the sediment depth column.

Although available field data for the solutes are included in the resulting figures (Figures 2–10) below just to provide a qualitative visual comparison with model predictions, any recalibration of the model parameters to fit field data is not considered in this study. Field data, wherever available, are included in the presented figures merely to provide a visual comparison with simulation predictions, where the presented model is not intended to reproduce the measured data, but the goal is to investigate and understand the impact of colloidal Fe (hydr)oxide transport on important biogeochemical processes operating in low-flow-velocity conditions in a natural subsurface environmental setting.

3.1 | Impact of hydrodynamic conditions on colloidal transport

Comparative simulations demonstrating the biogeochemical cycling of metals in lake sediments considering colloidal vs. immobile phases of Fe (hydr)oxide minerals using four different flow velocities (colored lines), as well as pure diffusive transport (black lines) cases are presented in Figures 2–6. In the figures, all solid lines correspond to colloidal HFO cases, whereas dashed lines correspond to immobile phases of HFO, with solutes traveling at corresponding flow velocities (or with pure diffusive transport as indicated by black lines). In general, the implementation of colloidal HFO cases indicated a significant difference in results when advective transport of solutes (and HFO) is considered in the system, as opposed to pure diffusive transport. The simulations demonstrate the strong impact of hydrochemical conditions, especially pH, on the mobility of heavy metals, particularly adsorption–desorption and precipitation–dissolution reactions. The implementation of EDL that compensates for the surface charge of HFO also plays a significant role on the mobility and dynamics of heavy metals in the system, as only the water within the macroporosity domain moves

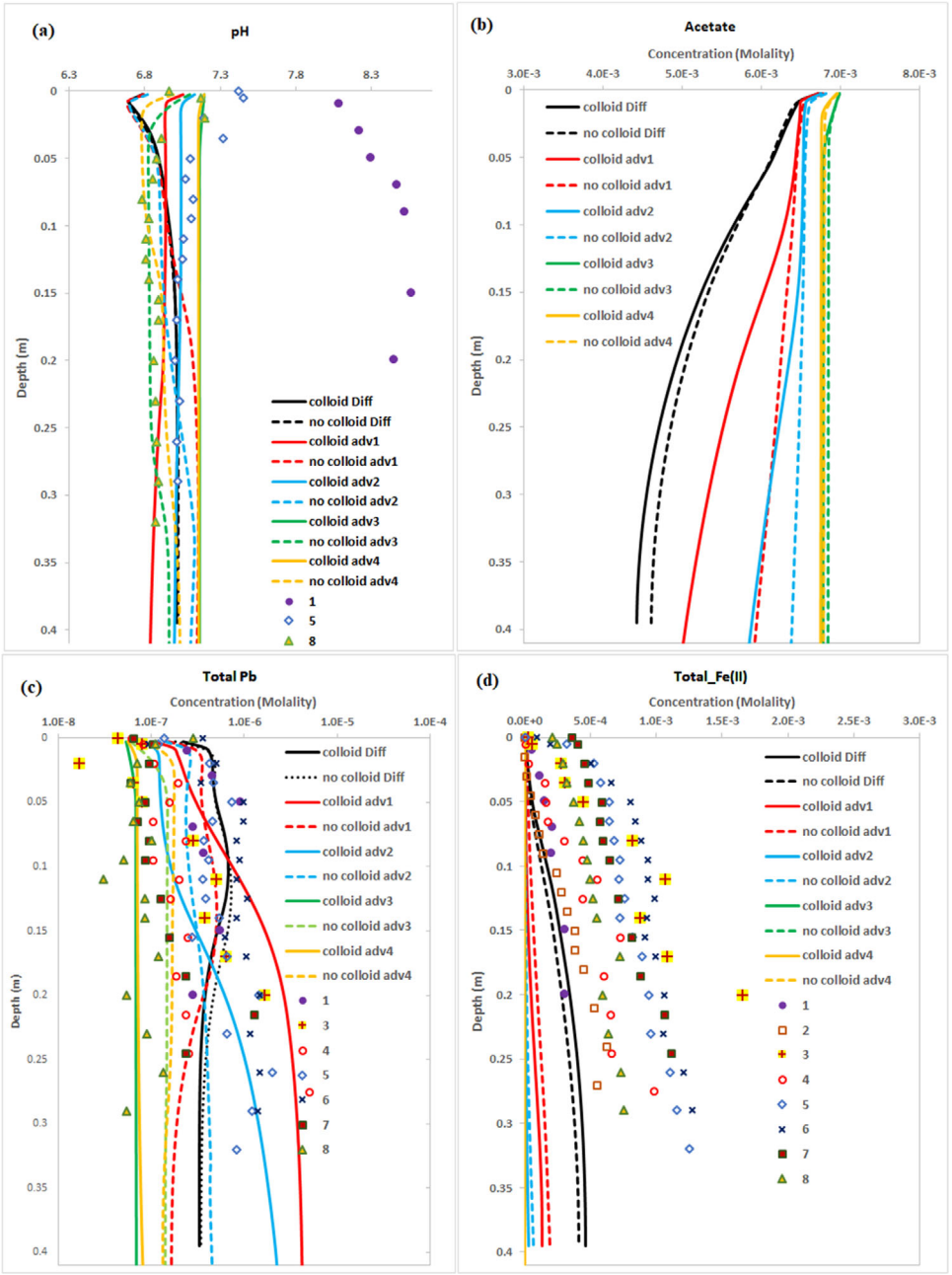

FIGURE 2 Comparison of colloidal vs. immobile (no colloid) implementation of hydrous ferric oxide particles on main aqueous species (pH, acetate, total Pb, and total Fe^{+2}) as a function of sediment depth with 50% electrostatic double layer. Lines represent model simulations. Simulations include diffusive transport (black lines) and advective transport with various flow velocities (colored lines). Symbols show measured data points compiled from various sources (data sources are discussed in Şengör, Spycher, Ginn, Sani, et al. 2007)

in response to a gradient. Therefore, the transport of ions in the macroporosity domain with the consideration of mobile vs. immobile HFO particles exerts a strong control on the overall release and transport of heavy metals in the system. Comparative concentrations of ions in the microporosity and macroporosity subdomains are also provided below to shed light on the discussions to explain the complex interplay of competing reactions.

The cause and impact of pH trends on the overall system dynamics is explained first. As discussed by Şengör et al. (2007a, 2007b), the pH trends are controlled by two main microbial processes: Fe reduction by FRB and sulfate reduction by SRB. The microbially mediated reductive dissolution of Fe (hydr)oxide minerals results in an increase in pH as shown by

$$8Fe(OH)_{3(s)} + CH_3COOH + 14H^+ \rightleftharpoons 8Fe^{2+} + 2HCO_3^- + 20H_2O \quad (8)$$

whereas upon shifting from suboxic to anoxic conditions at about 10-cm depth, microbially mediated sulfate reduction

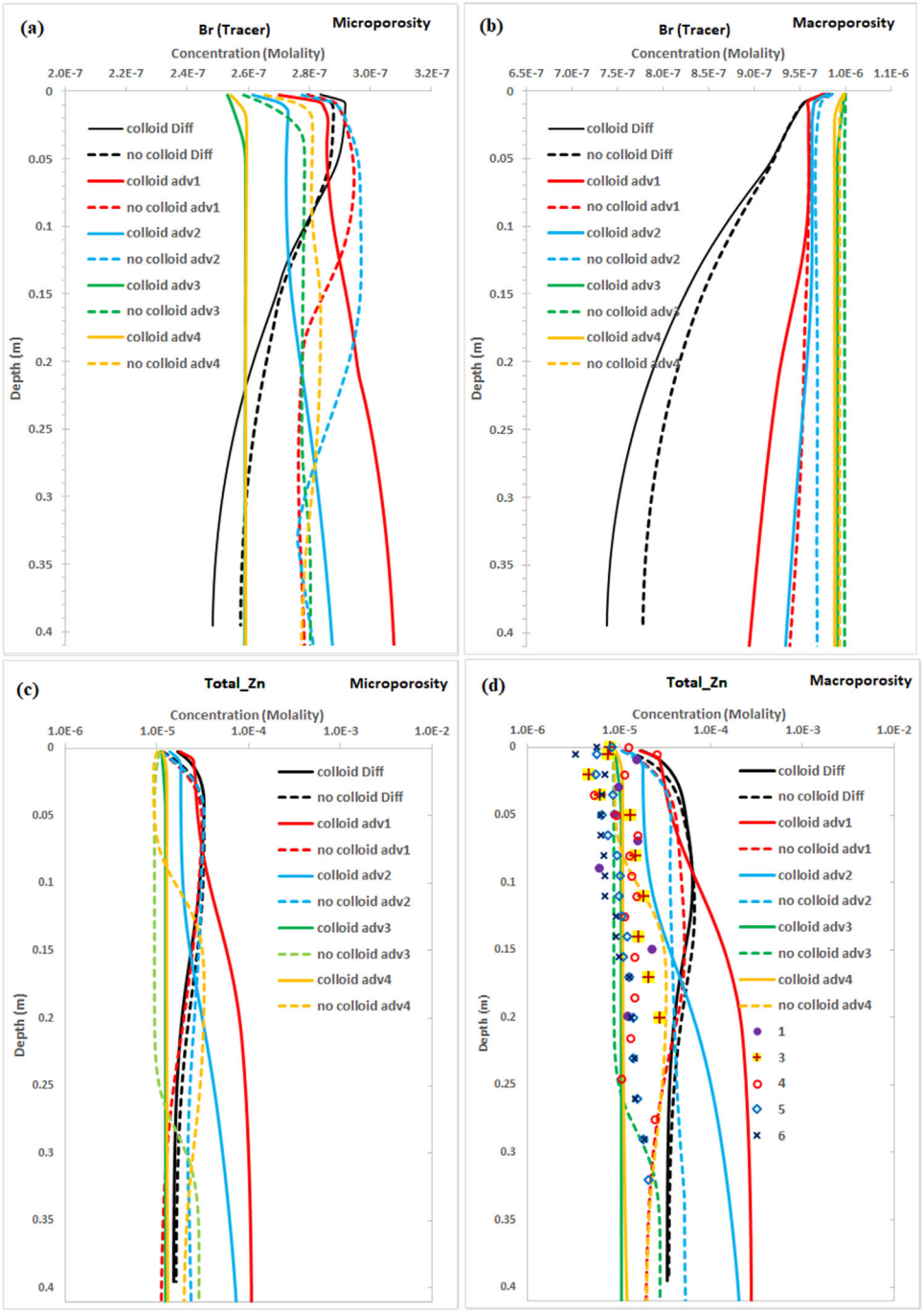

FIGURE 3 Comparison of colloidal vs. immobile (no colloid) implementation of hydrous ferric oxide particles on aqueous species [Br(tracer) and total Zn] within the macroporosity and microporosity subdomains as a function of sediment depth with 50% electrostatic double layer. Lines represent model simulations. Simulations include diffusive transport (black lines) and advective transport with various pore velocities (colored lines). Symbols show measured data points compiled from various sources (data sources are discussed in Şengör, Spycher, Ginn, Sani, et al. 2007)

reaction results in a decrease in pH as shown by

$$CH_3COO^- + SO_4^{2-} \rightleftharpoons 2CO_3^{2-} + HS^- + 2H^+ \qquad (9)$$

The pH trend profiles of model simulation results are shown in Figure 2a (upper left). When simulation results are compared in general, the colloidal transport cases, especially under higher flow velocity conditions, do not result in a significant change in pH with depth, as the impact of microbial processes (which are taking place relatively slowly) are less pronounced under high-flow conditions. Due to the initial boundary effect (i.e., equilibration of the initial solution with HFO sites at the initial boundary), initial pH values at the at top boundary start with higher pH values when

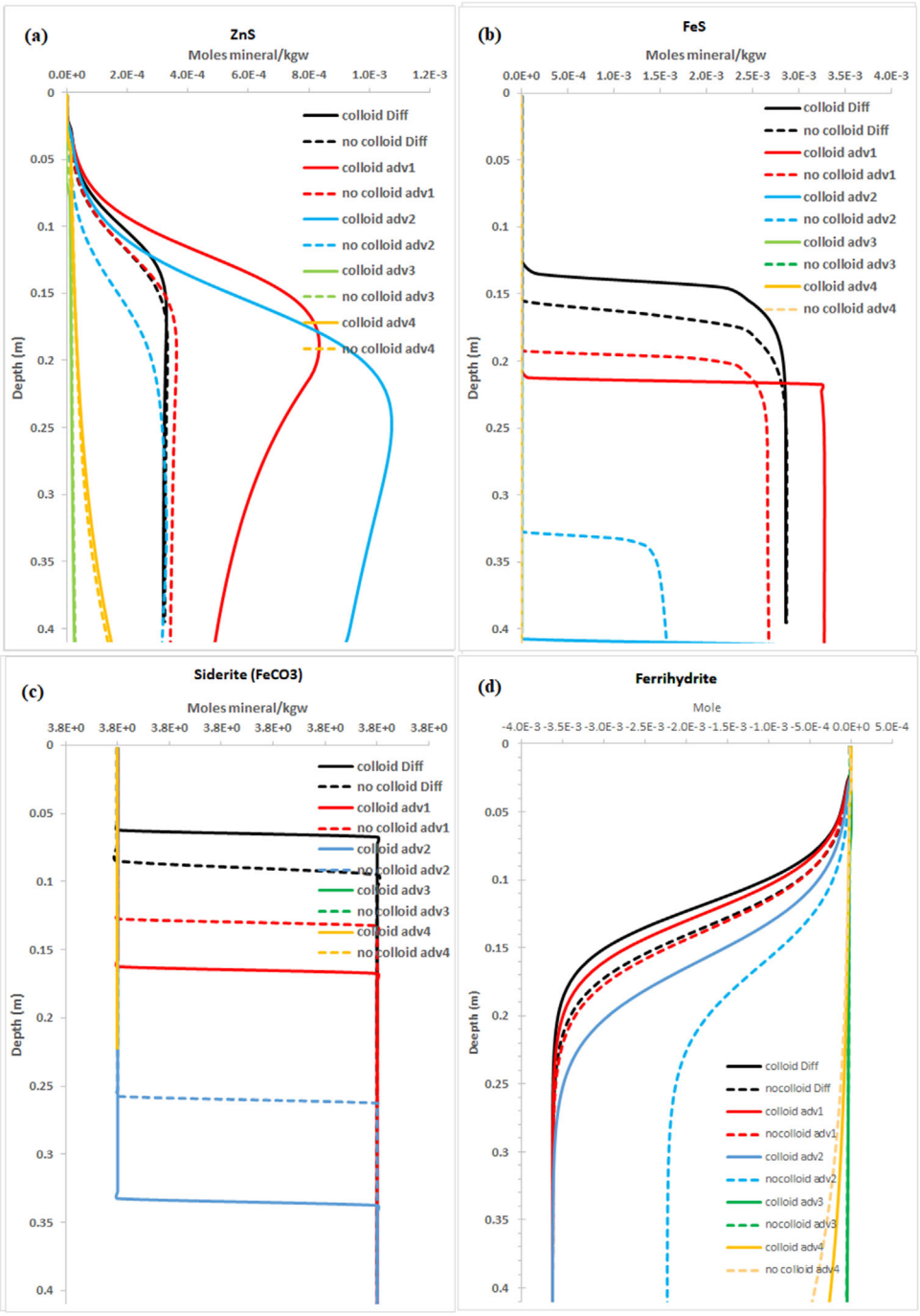

FIGURE 4 Comparison of colloidal vs. immobile (no colloid) implementation of hydrous ferric oxide particles on ZnS, FeS siderite ($FeCO_3$), and ferrihydrite minerals as a function of sediment depth with 50% electrostatic double layer. Lines represent model simulations. Simulations include diffusive transport (black lines) and advective transport with various pore velocities (colored lines). Symbols show measured data points compiled from various sources (data sources are discussed in Şengör, Spycher, Ginn, Sani, et al. 2007)

HFO phases are considered to be mobile. For immobile HFO cases, pH trends vary with depth as the microbial processes show prevailing impact with advective transport. At low-flow-velocity conditions, especially as the low Fe reduction rate (i.e., $V_m^{Fe3+} = 3 \times 10^{-12}$ s^{-1}, see Table 5) becomes comparable with advective transport velocities, the impact of immobile HFO surface interactions becomes significantly visible with increasing pH trends with depth, indicating the enhanced control of Fe reduction by FRB with immobile Fe (hydr)oxide mineral surfaces. The higher concentration of Fe(II) ions in parallel due to the enhanced microbial reductive dissolution reaction is seen in Figure 2d (lower right; compare colloidal [solid] lines with immobile [dashed] simulation results).

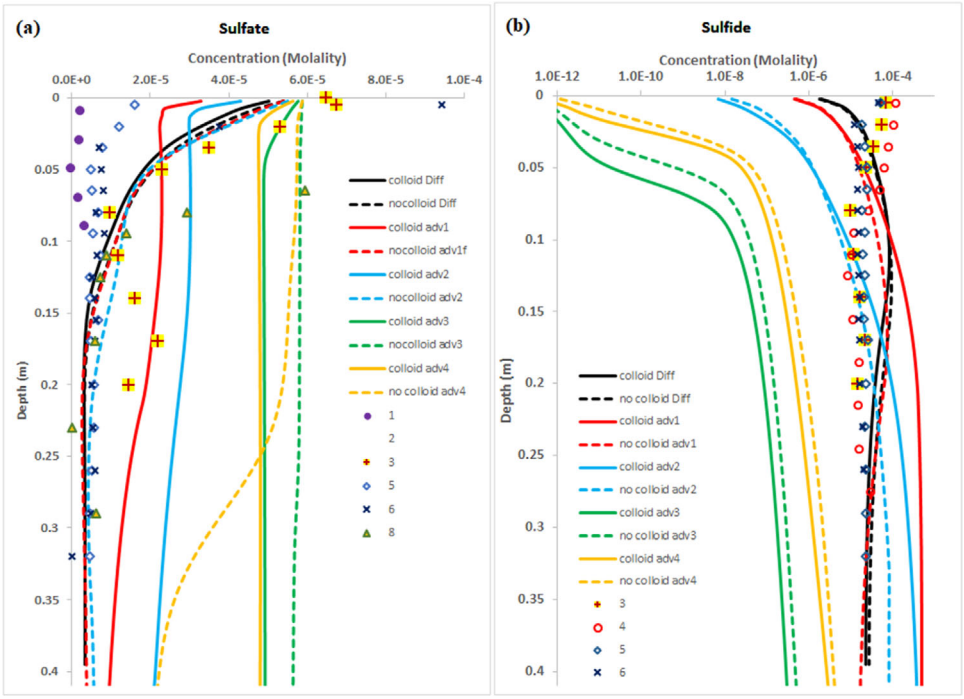

FIGURE 5 Comparison of colloidal vs. immobile (no colloid) implementation of hydrous ferric oxide particles on aqueous S species and sulfate species as a function of sediment depth with 50% electrostatic double layer. Lines represent model simulations. Simulations include diffusive transport (black lines) and advective transport with various pore velocities (colored lines). Symbols show measured data points compiled from various sources (data sources are discussed in Şengör, Spycher, Ginn, Sani, et al. 2007)

The response of the ions in the system to changes in pH (within both microporosity and macroporosity domains) is first demonstrated by comparing the adsorption–desorption behavior of a conservative tracer (Br) in the system under various flow velocities with mobile vs. immobile HFO cases. Figure 3 (a and b) shows the flushing of the sediment column with a hypothetical 1×10^{-6} M Br concentration that is introduced at the upper boundary (initial concentration within the column is 0). The model results show that at lower pH (occurring at the first around 10-cm sediment depth), Br ions are rather attracted to the microporosity domain due to the positive charge of the ferrihydrite surface below pzc ($pH_{PZC}^{HFO} = 8.11$). However, with the increase in pH towards the deeper depths, the accumulated Br ions in the microporosity domain are kicked out of the ferrihydrite surface to be replaced by hydroxyl ions, transferring to the macroporosity domain (as expected and discussed by J. Li & Şengör, 2020).

The dynamics of ion transfer within the EDL domains, combined with advective transport effects, result in significant differences in heavy metal profiles with sediment depth under colloidal vs. immobile HFO cases. When HFO particles are considered to be immobile, the enhanced Fe reduction results in the enhanced desorption of heavy metal ions from the colloidal surface, which then form strong aqueous metal (bi)sulfide complexes (in the form of Zn-HS, Pb-HS) after the production of biogenic sulfide by SRB in the anoxic zone. These negatively charged ions are kicked out of the ferrihydrite surface with the increase in pH, which are then transported down the depth of the sediment column along with the advective flow of water, ending up in lower heavy metal concentration profiles with depth. The lower amounts of heavy metals and aqueous sulfide ions in the system result in lower ZnS and PbS precipitation amounts towards the depth (Figure 4). The parallel decrease in sulfide concentrations are seen in Figure 5 (see immobile [dashed] lines). On the other hand, in the case of colloidal HFO, although the lower amount of Fe(II) ions are produced with lower amounts or desorbed heavy metals as a result of Fe reduction from mobile colloidal surfaces (compared with immobile colloidal surfaces), the produced heavy metals forming strong aqueous metal (bi)sulfide complexes are more retained in the system. At lower pH values, these ions are more attracted to the microporosity layer, and with transfer between the two domains (due to equilibrium between the microporosity and macroporosity subdomains), high concentrations of these ions are being observed in the free water, as more and more Fe reduction takes place from freshly arriving colloidal Fe (hydr)oxide mineral particles from the top boundary transporting through the sediment column with depth. As a result, higher heavy metal concentrations, as well as greater metal-sulfide precipitates (ZnS and PbS precipitates being formed as equilibrium metal and sulfide concentrations favor their precipitation) are being observed under colloidal HFO particle implementation. Therefore, these results reveal that when the potential

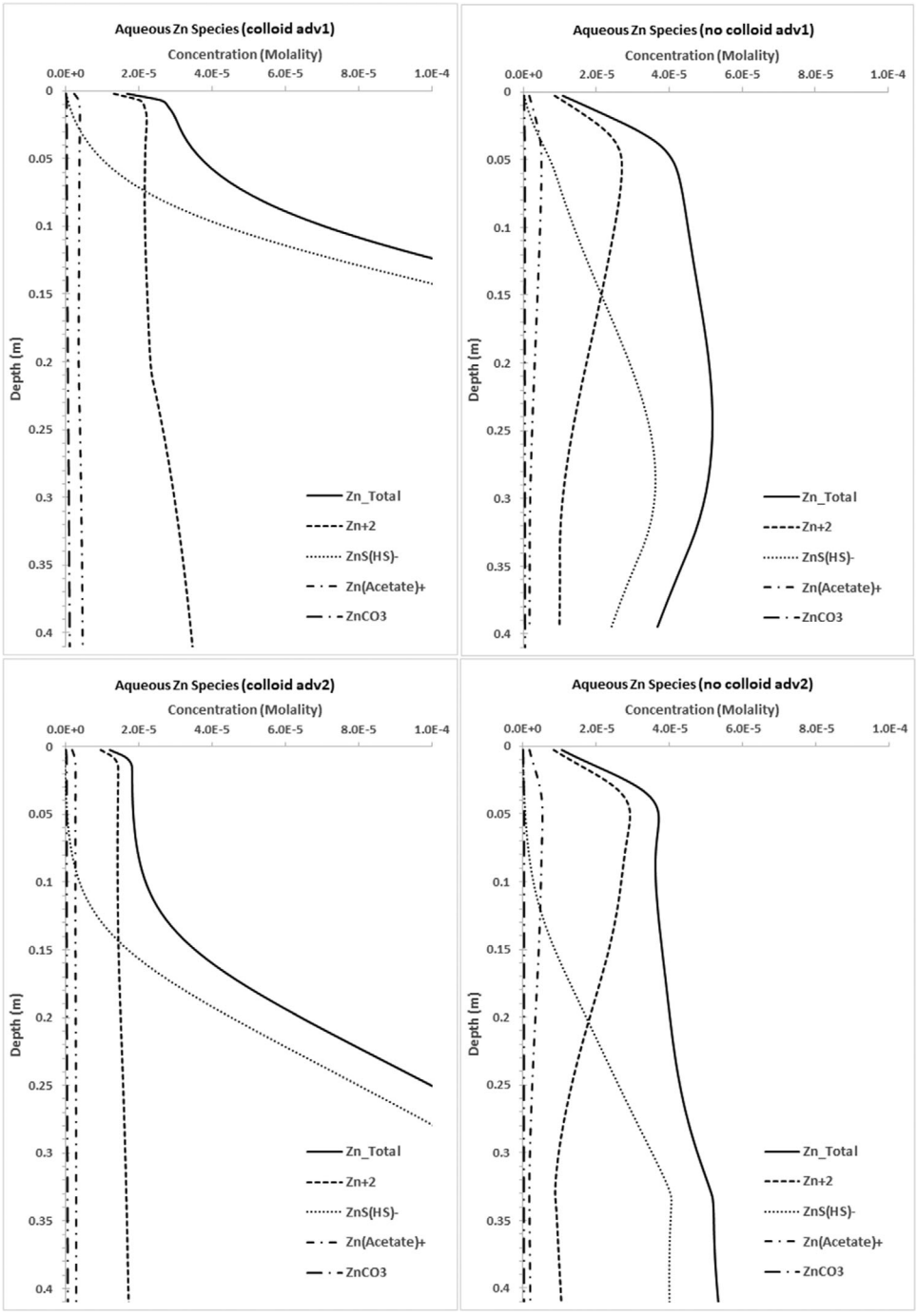

FIGURE 6 Calculated distributions of aqueous Zn species as a function of sediment depth: comparison of model predictions for mobile (colloid) vs. immobile (no colloid) implementation of hydrous ferric oxide particles with 50% electrostatic double layer. Simulations include advective transport with low flow water velocities adv1 (9×10^{-9} m s^{-1}) and adv2 (3×10^{-8} m s^{-1})

transport of sorbed contaminants (such as heavy metals) with colloidal sorbent particles is ignored, the contaminant concentrations in aqueous environments might be underestimated, especially under low-flow-velocity conditions (around 10^{-8} or 10^{-9} m s^{-1}). The amount of underestimation for dissolved heavy metals in the solution may go up to around 90% with depth, as a worst-Case-scenario condition at the lowest bound of low-flow-velocity situations (compare red solid and red dashed lines towards sediment depth in Figures 2c and 3d). This colloidal transport impact, however, may be less significant under higher flow velocity cases, even around the higher bound of low velocity environments (around 10^{-7} m s^{-1}). When pure diffusive transport case is considered, simulation results did not show much difference between colloidal vs. immobile HFO particle implementations in the system.

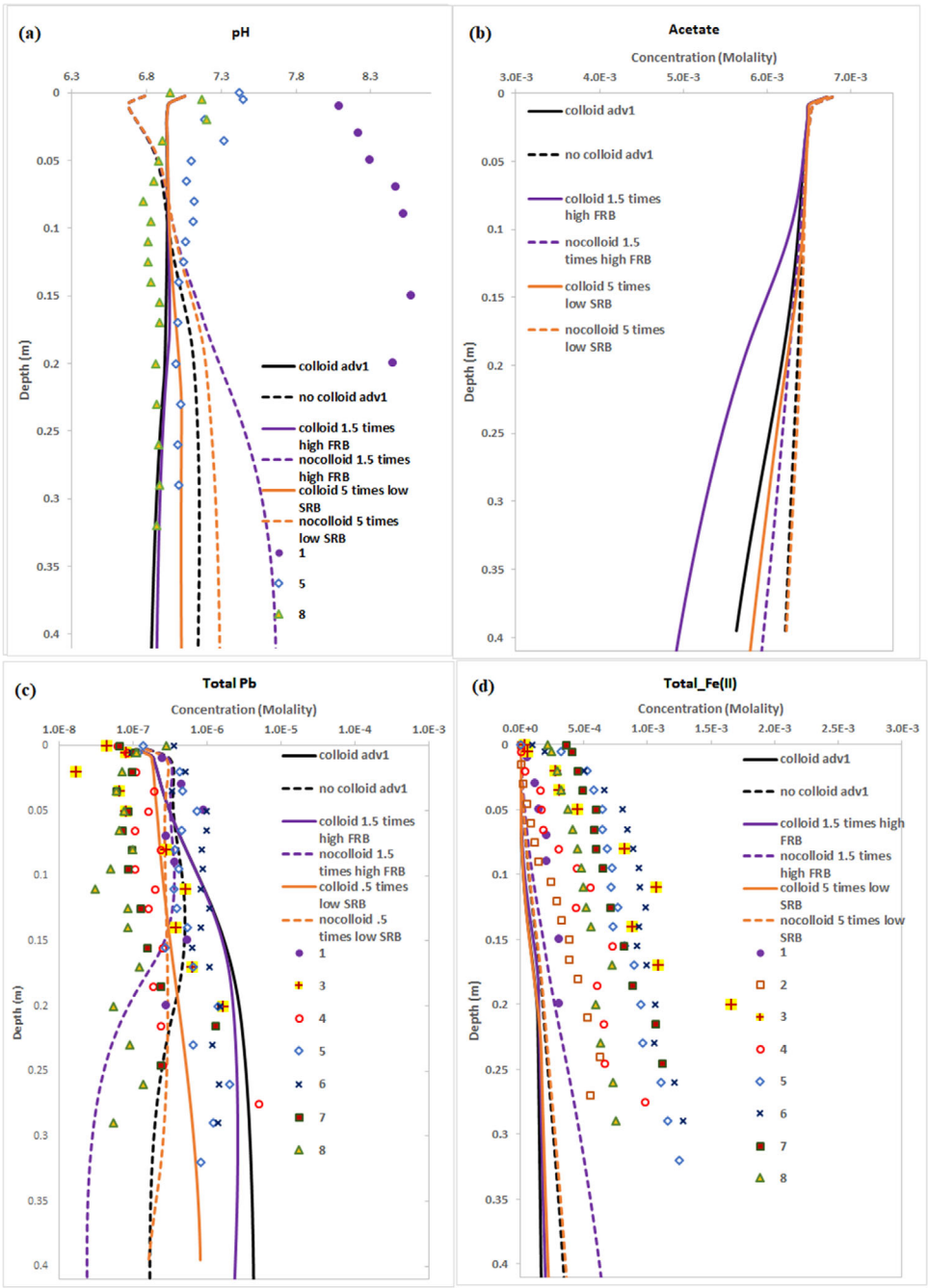

FIGURE 7 Comparison of colloidal vs. immobile (no colloid) implementation of hydrous ferric oxide (HFO) particles on main aqueous species (pH, acetate, total Pb, and total Fe^{+2}) as a function of sediment depth. Lines represent model simulations. Simulations also include predictions for "low" and "high" rates of sulfate-reducing bacteria (SRB, orange lines) and Fe-reducing bacteria (FRB, purple lines) activity rates when colloidal HFO particles are implemented with low flow water velocity adv1 (9×10^{-9} m s^{-1}) Symbols show measured data points compiled from various sources (data sources are discussed in Şengör, Spycher, Ginn, Sani, et al. 2007)

3.2 | Comparison of colloidal transport with different microbial process rates

To further illustrate the impact of pH and microbially mediated reaction kinetics on the overall dynamics of heavy metals under low-velocity-flow conditions, colloidal vs. immobile HFO particle implementation runs have been extended to test "high" and "low" rates of Fe(III) and sulfate reduction, respectively, with the low-advective-velocity transport (i.e., adv1 = 9×10^{-9} m s^{-1}). The "high" rate of Fe(III) reduction by FRB is tested as 1.5 times higher than the original reduction rate (i.e., $V_m^{Fe3+} = 3 \times 10^{-12}$ s^{-1}); and the "low" rate of sulfate reduction is tested as 5 times lower than the original reduction rate (i.e., $V_m^{SO42-} = 3 \times 10^{-9}$ s^{-1}) given in Table 5. Simulation results for pH and main ions are provided in Figures 7 and 8. Computed amounts of precipitated minerals

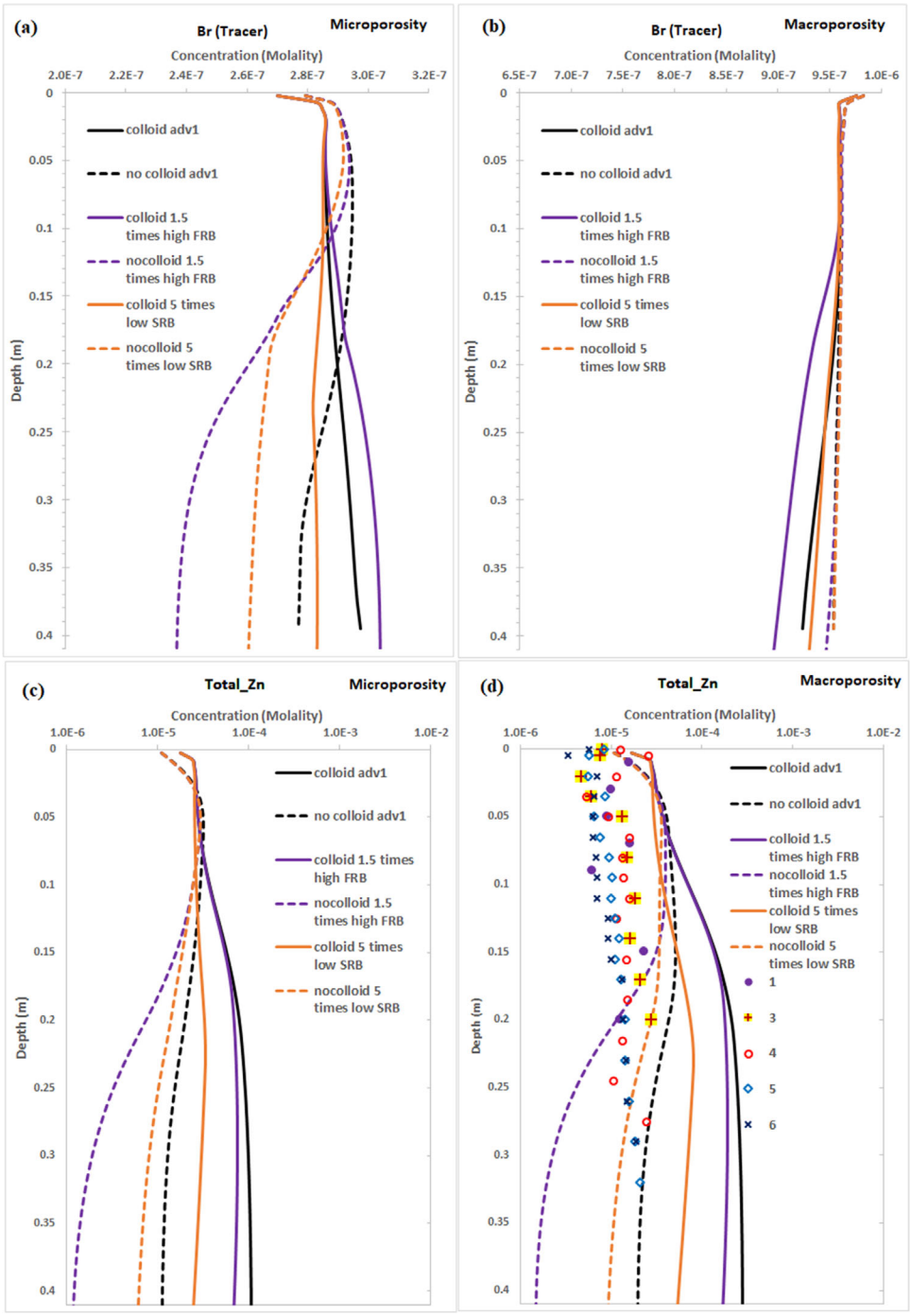

FIGURE 8 Comparison of colloidal vs. immobile (no colloid) implementation of hydrous ferric oxide (HFO) particles on aqueous species [Br(tracer) and total Zn] within the macroporosity and microporosity subdomains as a function of sediment depth with 50% electrostatic double layer. Lines represent model simulations. Simulations also include predictions for "low" and "high" rates of sulfate-reducing bacteria (SRB, orange lines) and Fe-reducing bacteria (FRB, purple lines) activity rates when colloidal HFO particles are implemented with low flow water velocity adv1 (9×10^{-9} m s^{-1}) Symbols show measured data points compiled from various sources (data sources are discussed in Şengör, Spycher, Ginn, Sani, et al. 2007)

are given in Figure 9. Again, the solid lines correspond to the colloidal HFO cases, whereas dashed lines correspond to immobile HFO particle runs. Competitive effects of varying Fe and sulfate reduction rates on the pH trends, and release and transport of heavy metals in the system with the consideration of colloidal vs. immobile HFO particles, are discussed below.

The reactive transport model results show that when Fe reduction rate is increased, the increase in pH (due to Equation 8 as given above) is further pronounced in the

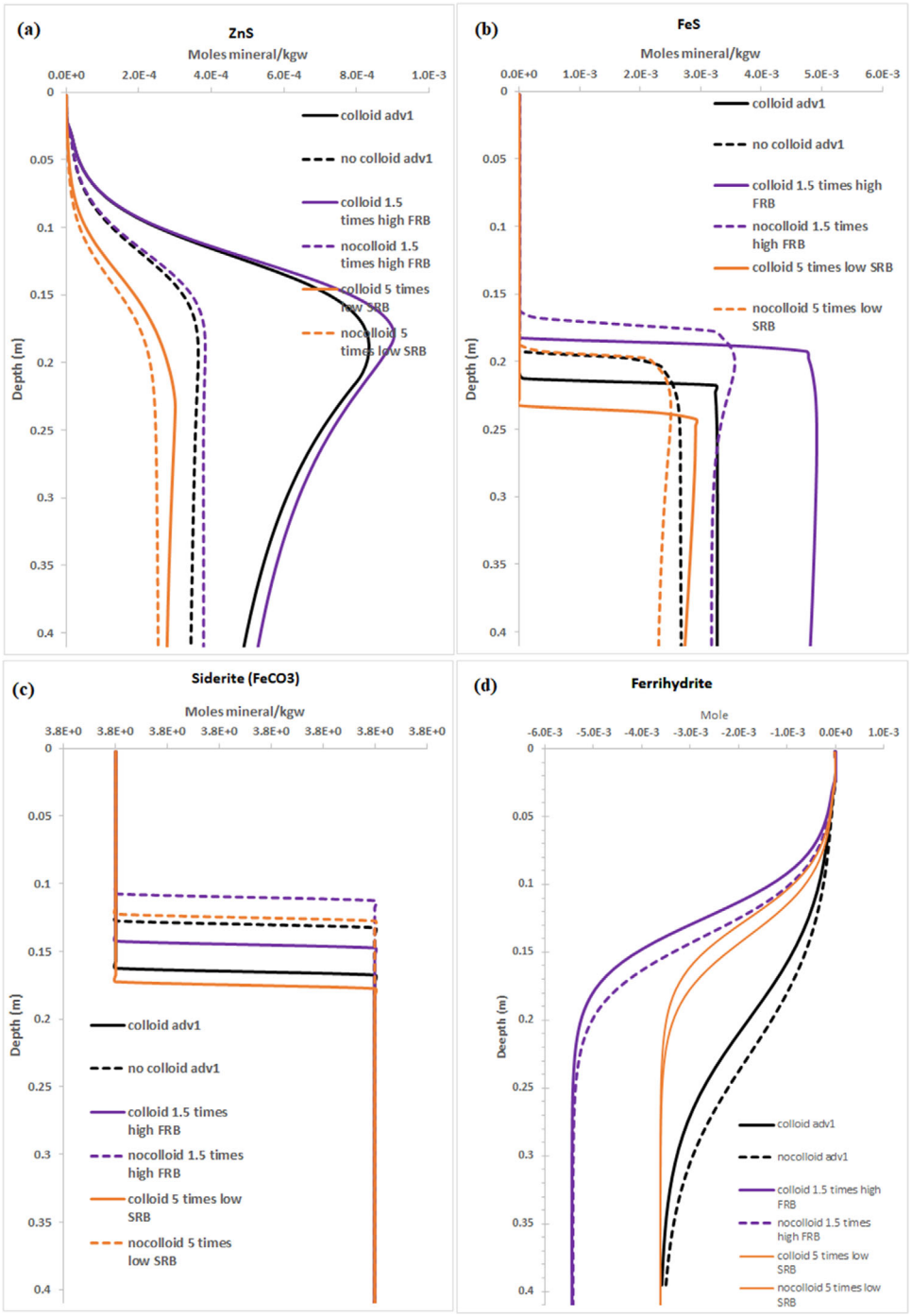

FIGURE 9 Comparison of colloidal vs. immobile (no colloid) implementation of hydrous ferric oxide (HFO) particles on ZnS, FeS siderite ($FeCO_3$), and ferrihydrite minerals as a function of sediment depth with 50% electrostatic double layer. Lines represent model simulations. Simulations also include predictions for "low" and "high" rates of sulfate-reducing bacteria (SRB, orange lines) and Fe-reducing bacteria (FRB, purple lines) activity rates when colloidal HFO particles are implemented with low flow water velocity adv1 (9×10^{-9} m s^{-1}) Symbols show measured data points compiled from various sources (data sources are discussed in Şengör, Spycher, Ginn, Sani, et al. 2007)

case of immobile HFO particle implementation, resulting in very high pH profile trends with depth (blue dashed lines in Figure 7). This high pH trends correspond with further desorption of metal ions [with accompanying increase in Fe(II) levels as a result of microbial Fe reduction], and increased aqueous metal (bi)sulfide complexes, which are transported and "washed out" from the solution domain by advective transport of solutes in the free-water domain. This results in further decreases in heavy metal ions in the solution along with further decreased aqueous sulfide ions (Figures 8

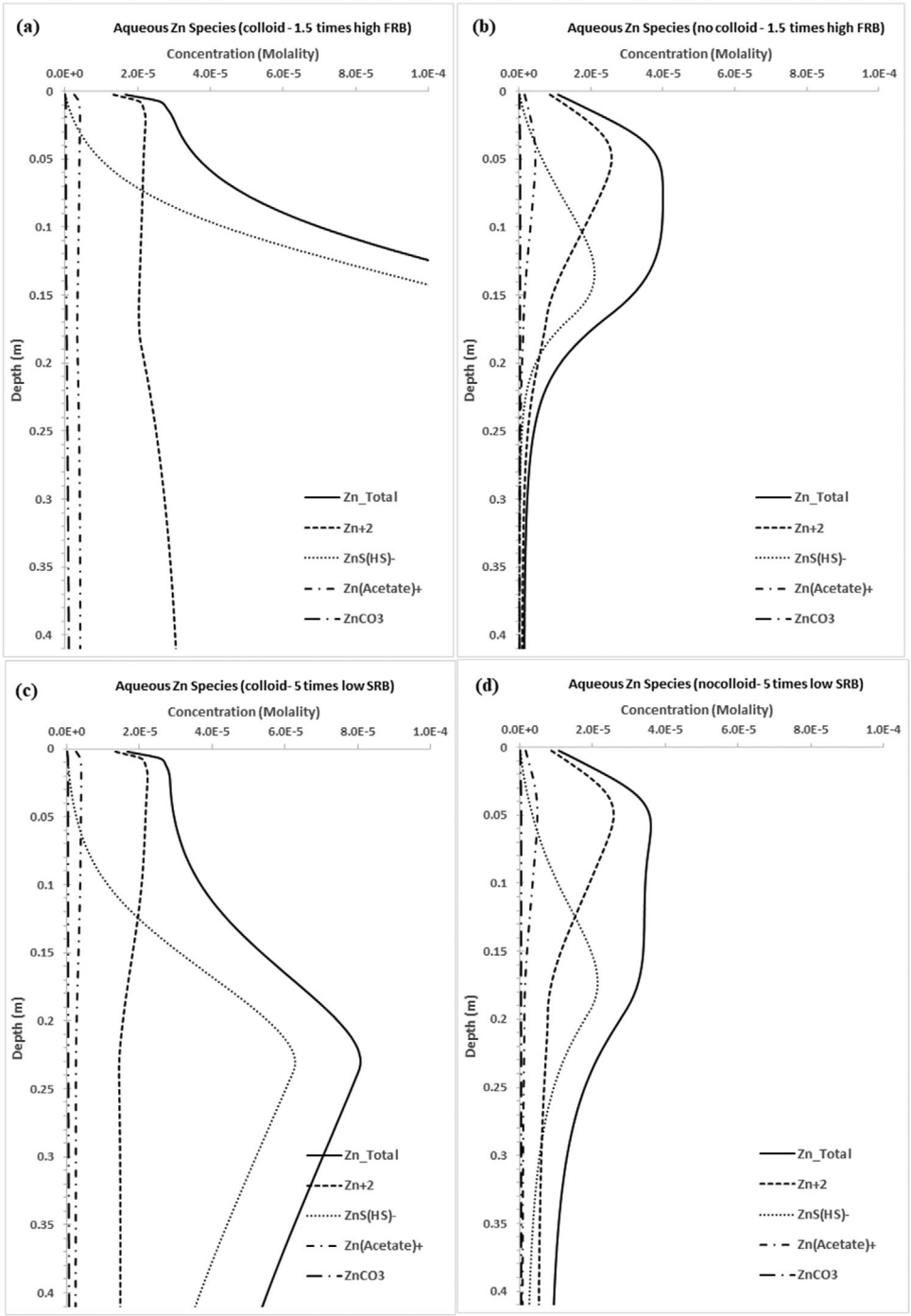

FIGURE 10 Calculated distributions of aqueous Zn species as a function of sediment depth: comparison of model predictions for mobile (colloid) vs. immobile (no colloid) implementation of hydrous ferric oxide (HFO) particles with 50% electrostatic double layer. Simulations include predictions for "low" and "high" rates of sulfate-reducing bacteria (SRB) and Fe-reducing bacteria (FRB) activity rates when colloidal HFO particles are implemented with low flow water velocity adv1 (9×10^{-9} m s^{-1})

and 10). The amounts of ZnS and PbS precipitate formation do not change significantly though, due to the already low amounts of metal and sulfide ions remaining in the medium. As a result of high Fe(II) production, FeS precipitation forms earlier but with lower amounts compared with the colloidal HFO case results (Figure 9). If the sulfate reduction rate is lowered, on the other hand, then pH increases due to the lower amount of sulfide production (red lines in Figure 7), which results in lower amounts of ZnS and PbS precipitate formation and lower concentrations of heavy metal ion profiles in the system. The lower amounts of sulfide production also lower the potential of strong aqueous metal (bi)sulfide

complex formation. When HFO particles are considered to be mobile, again relatively high amounts of heavy metal ions remain in solution compared with the immobile HFO case. Comparing the relative impacts of "high" and "low" rates of Fe and sulfate reduction, the system dynamics are observed to be highly sensitive to Fe reduction compared with sulfate reduction, as also previously noted by J. Li and Şengör, 2020. This sensitivity of Fe reduction on the overall biogeochemical dynamics of the system is shown to be further more visible in the colloidal vs. immobile HFO implementation, as demonstrated in this study. Although enhanced Fe reduction impacts on the pH and metal mobilization dynamics are observed in the immobile HFO particle runs, increased heavy metal concentrations are retained in the system as a result of the net effect of biogeochemical reactions in the presence of colloidal HFO, as opposed to low concentration profiles with immobile HFO. This opposing impact of heavy metal release and transport is observed to be highly pronounced especially under low-flow-velocity conditions (around 10^{-8} or 10^{-9} m s^{-1}) with strong sensitivity to low Fe reduction rates, commonly observed in anaerobic subsurface environments.

3.3 | Environmental consideration and significance

The modeling study demonstrates the impact of colloidal Fe (hydr)oxide transport on overall heavy metal dynamics with strong dependence of flow velocity on Fe reduction rates. Understanding the complex interplay between flow velocity impacts and colloidal transport along with coupled microbially mediated reactions—especially Fe-reduction—would be of utmost importance for effective management and (bio)remediation of subsurface and groundwater contaminated environments, as well as for predicting heavy metal transport through these environmental systems. The high reactivity of Fe nanoparticles, and their potential use as electron acceptors for microbial Fe reduction, can be of significant use for bioremediation applications for a variety of pollutants in the subsurface.

The outcomes of this modeling study have considerable implications for metal transport in low-advective-velocity subsurface systems such as transport through low-permeability clayey lenses enclosed in heterogeneous aquifer systems, leakage through aquitards overlaying confined aquifers, and leakage through compacted clay liners that are widely used as hydraulic barriers in landfills, underground storage tanks, vertical cutoff walls, and surface impoundments. As the impact of colloidal facilitated transport is observed to be more significant under low-flow-velocity conditions with enhanced pollutant (heavy-metal) concentrations observed in the system (as a result of the net effect of biogeochemical reactions in the presence of colloidal Fe-oxide based minerals), this would have opposing impacts depending on the specific subsurface environmental system of concern. For example, although for leakage through aquitards overlaying confined aquifers or leakage through compacted clay liners, this enhanced pollutant transport might have negative implications; on the other hand, it might have positive impacts with regards to effective management and/or (bio)remediation of subsurface and groundwater contaminated environments, especially for transport of pollutants through low-permeability clayey lenses enclosed in heterogeneous aquifer systems. Therefore, the impacts of colloidal transport of pollutants can be extended or used to help design strategies according to the intended desired use. For the design of compacted clay liners to be used for hydraulic barriers in landfills, underground storage tanks, vertical cutoff walls, or surface impoundments, the possibility of colloidal transport of, for example, Fe-based particles might be minimized or designed to be kept at minimum, whereas for effective remediation of low-permeability clayey lenses within heterogeneous aquifer systems, nanosized Fe oxide particles with high reactivity might be considered for use as electron acceptors for Fe reduction along with their colloidal transport. The model outcomes can also be used to consider modeling or predicting possible leakage or pollutant transport through the low-flow-velocity settings, or be integrated with colloidal transport dynamics in the system for prediction purposes or risk assessment models for subsurface systems.

The impact of colloidal load, as well as colloid type [Mn (hydr)oxide phases in addition to Fe (hydr)oxide particles], is currently being investigated and will be the subject of future work.

4 | SUMMARY AND CONCLUSIONS

In the present study, the impact of colloidal facilitated transport of heavy metals on the overall dynamics of biogeochemical processes in example diffusive transport-dominated lake sediments of LcdA is investigated. The impact of colloidal HFO particles on reactive transport and sorption of heavy metals in a natural environment, integrating a coupled biotic reaction network with multiple terminal electron acceptors, is presented. The results of the study reveal that when the potential transport of sorbed contaminants with colloidal particles is ignored, the contaminant concentrations in aqueous environments might be underestimated, especially under low-flow-velocity conditions (around 10^{-8} or 10^{-9} m s^{-1}), where the amount of underestimation for dissolved heavy metals may reach around 90% with depth, as a worst-case scenario at the lowest bound of low-flow-velocity situations. This colloidal transport impact, however, may be less significant in higher flow velocity cases, even around

the upper bound of low-velocity environments (around 10^{-7} m s^{-1}). The model results illustrate the sensitivity of the colloidal transport of contaminants to EDL implementation under low-flow-velocity advective transport conditions, especially when microbially mediated Fe reduction rates become comparable with advective transport velocities in the system. The outcomes of this modeling study may have significant implications for pollutant (e.g. heavy-metal) transport in low-advective-velocity subsurface systems. Considering leakage through aquitards (e.g., overlaying confined aquifers or leakage through compacted clay liners), the enhanced pollutant transport might have negative impacts, whereas it might have positive considerations regarding pollutant removal through low-permeability clayey lenses within heterogeneous aquifer systems. Therefore, the model outcomes can be helpful to shed light on any intended design strategies to be used accordingly or integrated with colloidal transport dynamics in the system for prediction purposes or risk assessment models for subsurface remediation.

ACKNOWLEDGMENTS

This publication/paper has been produced benefiting from the 2236 Co-Funded Brain Circulation Scheme2 (CoCirculation2) of TÜBİTAK (Project No. 120C053). However, the entire responsibility of the publication/paper belongs to the owner of the publication/paper. The financial support received from TÜBİTAK does not mean that the content of the publication is approved in a scientific sense by TÜBİTAK.

AUTHOR CONTRIBUTIONS

S. Sevinç Şengör: Conceptualization; Data curation; Formal analysis; Funding acquisition; Investigation; Methodology; Project administration; Resources; Visualization; Writing – original draft; Writing – review & editing. Kahraman Ünlü: Data curation; Supervision; Writing – review & editing.

CONFLICT OF INTEREST

The authors declare no conflict of interest.

ORCID

S. Sevinç Şengör https://orcid.org/0000-0003-3944-1172

REFERENCES

Alonso, U., Missana, T., Patelli, A., Rigato, V., & Ravagnan, J. (2007). Colloid diffusion in crystalline rock: An experimental methodology to measure diffusion coefficients and evaluate colloid size dependence. *Earth and Planetary Science Letters*, *259*(3–4), 372–383. https://doi.org/10.1016/j.epsl.2007.04.042

Alt-Epping, P., Tournassat, C., Rasouli, P., Steefel, C. I., Mayer, K. U., Jenni, A., Mäder, U., Sengor, S. S., & Fernández, R. (2015). Benchmark reactive transport simulations of a column experiment in compacted bentonite with multispecies diffusion and explicit treatment of electrostatic effects. *Computational Geosciences*, *19*(3), 535–550. https://doi.org/10.1007/s10596-014-9451-x

Amde, M., Liu, J.-F., Tan, Z., & Bekana, D. (2017). Transformation and bioavailability of metal oxide nanoparticles in aquatic and terrestrial environments. A review. *Environmental Pollution*, *230*, 250–267. https://doi.org/10.1016/j.envpol.2017.06.064

Appelo, C. A. J., Van Loon, L. R., & Wersin, P. (2010). Multicomponent diffusion of a suite of tracers (HTO, Cl, Br, I, Na, Sr, Cs) in a single sample of Opalinus clay. *Geochimica et Cosmochimica Acta*, *74*(4), 1201–1219. https://doi.org/10.1016/j.gca.2009.11.013

Appelo, C. A. J., Vinsot, A., Mettler, S., & Wechner, S. (2008). Obtaining the porewater composition of a clay rock by modeling the in-and out-diffusion of anions and cations from an in-situ experiment. *Journal of Contaminant Hydrology*, *101*(1), 67–76. https://doi.org/10.1016/j.jconhyd.2008.07.009

Appelo, C. A. J., & Wersin, P. (2007). Multicomponent diffusion modeling in clay systems with application to the diffusion of tritium, iodide, and sodium in Opalinus clay. *Environmental Science & Technology*, *41*(14), 5002–5007. https://doi.org/10.1021/es0629256

Arora, B., Şengör, S. S., Spycher, N. F., & Steefel, C. I. (2015). A reactive transport benchmark on heavy metal cycling in lake sediments. *Computational Geosciences*, *19*(3), 613–633. https://doi.org/10.1007/s10596-014-9445-8

Bard, A. J., & Faulkner, L. R. (2001). *Electrochemical methods: Fundamentals and applications* (2nd ed.). Wiley.

Bekhit, H. M., El-Kordy, M. A., & Hassan, A. E. (2009). Contaminant transport in groundwater in the presence of colloids and bacteria: model development and verification. *Journal of Contaminant Hydrology*, *108*(3), 152–167. https://doi.org/10.1016/j.jconhyd.2009.07.003

Bekhit, H. M., Hassan, A. E., Harris-Burr, R., & Papelis, C. (2006). Experimental and numerical investigations of effects of silica colloids on transport of strontium in saturated sand columns. *Environmental Science & Technology*, *40*(17), 5402–5408. https://doi.org/10.1021/es060333h

Benhabib, K., Simonnot, M. O., Faure, P., & Sardin, M. (2017). Evidence of colloidal transport of PAHs during column experiments run with contaminated soil samples. *Environmental Science and Pollution Research*, *24*(10), 9220–9228. https://doi.org/10.1007/s11356-017-8586-4

Bennacer, L., Ahfir, N. D., Alem, A., & Wang, H. (2017). Coupled effects of ionic strength, particle size, and flow velocity on transport and deposition of suspended particles in saturated porous media. *Transport in Porous Media*, *118*(2), 251–269. https://doi.org/10.1007/s11242-017-0856-6

Bin, G., Cao, X., Dong, Y., Luo, Y., & Ma, L. Q. (2011). Colloid deposition and release in soils and their association with heavy metals. *Critical Reviews in Environmental Science and Technology*, *41*(4), 336–372. https://doi.org/10.1080/10643380902871464

Borgnino, L. (2013). Experimental determination of the colloidal stability of Fe (III)-montmorillonite: Effects of organic matter, ionic strength and pH conditions. *Colloids and Surfaces A: Physicochemical and Engineering Aspects*, *423*, 178–187. https://doi.org/10.1016/j.colsurfa.2013.01.065

Bourikas, K., Hiemstra, T., & van Riemsdijk, W. H. (2001). Ion pair formation and primary charging behavior of titanium oxide (anatase and rutile). *Langmuir*, *17*(3), 749–756. https://doi.org/10.1021/la000806c

Bradford, S. A., Yates, S. R., Bettahar, M., & Šimůnek, J. (2002). Physical factors affecting the transport and fate of colloids in saturated porous media. *Water Resources Research*, *38*(12), xx–xx. https://doi.org/10.1029/2002WR001340

Braunschweig, J., Klier, C., Schröder, C., Händel, M., Bosch, J., Totsche, K. U., & Meckenstock, R. U. (2014). Citrate influences microbial Fe hydroxide reduction via a dissolution–disaggregation mechanism. *Geochimica et Cosmochimica Acta*, *139*, 434–446. https://doi.org/10.1016/j.gca.2014.05.006

Brugato, C. (1999). *Mathematical modeling of an anaerobic syntrophic butyrate-degrading coculture* [Master's thesis, University California, Davis].

Buil, B. (2002). *Caracterización petrológica, mineralógica, geoquímica y evaluación del comportamiento geoquímico de las REE en la fase sólida (granitoides y rellenos fisurales) del sistema de interacción agua-roca del entorno de la Mina Ratones* (Technical Publication PT-07-02). ENRESA.

Cheng, D., Liao, P., & Yuan, S. (2016). Effects of ionic strength and cationic type on humic acid facilitated transport of tetracycline in porous media. *Chemical Engineering Journal*, *284*, 389–394. https://doi.org/10.1016/j.cej.2015.08.159

de Jonge, L. W., Kjærgaard, C., & Moldrup, P. (2004). Colloids and colloid-facilitated transport of contaminants in soils. *Vadose Zone Journal*, *3*(2), 321–325. https://doi.org/10.2136/vzj2004.0321

Doussan, C., Poitevin, G., Ledoux, E., & Detay, M. (1997). River bank filtration: Modelling of the changes in water chemistry with emphasis on nitrogen species. *Journal of Contaminant Hydrology*, *25*, 129–156. https://doi.org/10.1016/S0169-7722(96)00024-1

Dzombak, D. A., & Morel, F. M. M. (1990). *Surface complexation modeling hydrous ferric oxide*. John Wiley & Sons.

Emerson, H. P., Hickok, K. A., & Powell, B. A. (2016). Experimental evidence for ternary colloid- facilitated transport of Th (IV) with hematite (α-Fe 2 O 3) colloids and Suwannee River fulvic acid. *Journal of Environmental Radioactivity*, *165*, 168–181. https://doi.org/10.1016/j.jenvrad.2016.10.001

Fatehah, M. O., Aziz, H. A., & Stoll, S. (2014). Nanoparticle properties, behavior, fate in aquatic systems and characterization methods. *Journal of Colloid Science and Biotechnology*, *3*(2), 111–140. https://doi.org/10.1166/jcsb.2014.1090

Ghiasi, B., Niksokhan, M. H., & Mahdavi Mazdeh, A. (2020a). Co-transport of chromium (VI) and bentonite colloidal particles in water-saturated porous media: Effect of colloid concentration, sand gradation, and flow velocity. *Journal of Contaminant Hydrology*, *234*, 103682. https://doi.org/10.1016/j.jconhyd.2020.103682

Ghiasi, B., Niksokhan, M. H., & Mahdavi Mazdeh, A. (2020b). Effect of bentonite particles' presence on two-dimensional chromium transmission. *Environmental Science and Pollution Research*, *27*, 21692–21701. https://doi.org/10.1007/s11356-020-08638-y

He, J., Wang, D., & Zhou, D. (2019). Transport and retention of silver nanoparticles in soil: effects of input concentration, particle size and surface coating. *Science of the Total Environment*, *648*, 102–108. https://doi.org/10.1016/j.scitotenv.2018.08.136

Hofmann, A., Pelletier, M., Michot, L., Stradner, A., Schurtenberger, P., & Kretzschmar, R. (2004). Characterization of the pores in hydrous ferric oxide aggregates formed by freezing and thawing. *Journal of Colloid and Interface Science*, *271*(1), 163–173. https://doi.org/10.1016/j.jcis.2003.11.053

Holmboe, M., Wold, S., & Jonsson, M. (2012). Porosity investigation of compacted bentonite using XRD profile modeling. *Journal of Contaminant Hydrology*, *128*(1–4), 19–32. https://doi.org/10.1016/j.jconhyd.2011.10.005

Jakob, A. (2004). *Matrix diffusion for performance assessment: Experimental evidence, modeling, assumptions and open questions*. Paul Scherrer Institut.

Javadi, S., Ghavami, M., Zhao, Q., & Bate, B. (2017). Advection and retardation of non-polar contaminants in compacted clay barrier material with organoclay amendment. *Applied Clay Science*, *142*, 30–39. https://doi.org/10.1016/j.clay.2016.10.041

Katzourakis, V. E., & Chrysikopoulos, C. V. (2015). Modeling dense-colloid and virus cotransport in three-dimensional porous media. *Journal of Contaminant Hydrology*, *181*, 102–113. https://doi.org/10.1016/j.jconhyd.2015.05.010

Kheirabadi, M., Niksokhan, M. H., & Omidvar, B. (2017). Colloid-associated groundwater contaminant transport in homogeneous saturated porous media: mathematical and numerical modeling. *Environmental Modeling & Assessment*, *22*(1), 79–90. https://doi.org/10.1007/s10666-016-9518-2

Kretzschmar, R., Borkovec, M., Grolimund, D., & Elimelech, M. (1999). Mobile subsurface colloids and their role in contaminant transport. *Advances in Agronomy*, *66*, 121–193. https://doi.org/10.1016/S0065-2113(08)60427-7

Li, J., & Şengör, S. S. (2020). Biogeochemical cycling of heavy metals in lake sediments: Impact of multispecies diffusion and electrostatic effects. *Computational Geosciences*, *24*(4), 1463–1482. https://doi.org/10.1007/s10596-019-09915-7

Li, X., Zhang, W., Qin, Y., Ma, T., Zhou, J., & Du, S. (2019). Fe–colloid cotransport through saturated porous media under different hydrochemical and hydrodynamic conditions. *Science of The Total Environment*, *647*, 494–506. https://doi.org/10.1016/j.scitotenv.2018.08.010

Litter, M. I., Quici, N., & Meichtry, M. (Eds.). (2018). *Iron nanomaterials for water and soil treatment*. CRC Press.

Ma, J., Guo, H., Lei, M., Li, Y., Weng, L., Chen, Y., & Xiu, W. (2017). Enhanced transport of ferrihydrite colloid by chain-shaped humic acid colloid in saturated porous media. *Science of The Total Environment*, *621*, 1581–1590. https://doi.org/10.1016/j.scitotenv.2017.10.070

Montalvo, D., & Smolders, E. (2019). Metals and metalloid removal by colloidal humic acid–goethite: Column experiments and geochemical modeling. *Vadose Zone Journal*, *18*(1), 1–9. https://doi.org/10.2136/vzj2019.01.0004

Ohlsonn, Y., & Neretnieks, I. (1997). *Diffusion data in granite: Recommended values* (SKB Technical Report TR-97-20). Stockholms Kooperativa Bostadsförening.

Parkhomenko, E. I. (1967). *Electrical properties of the rocks*. Plenum Press.

Parkhurst, D. L., & Appelo, C. A. J. (2013). *Description of input and examples for PHREEQC version 3: a computer program for speciation, batch-reaction, one-dimensional transport, and inverse geochemical calculations* (No. 6-A43). USGS.

Peng, S., Wu, D., Ge, Z., Tong, M., & Kim, H. (2017). Influence of graphene oxide on the transport and deposition behaviors of colloids in saturated porous media. *Environmental Pollution*, *225*, 141–149. https://doi.org/10.1016/j.envpol.2017.03.064

Roy, S. B., & Dzombak, D. A. (1997). Chemical factors influencing colloid-facilitated transport of contaminants in porous media. *Environmental Science & Technology*, *31*(3), 656–664. https://doi.org/10.1021/es9600643

Russell, E. W. (1973). *Soil conditions and plant growth*. Longmans Publishing.

Ryan, J. N., & Elimelech, M. (1996). Colloid mobilization and transport in groundwater. *Colloids and Surfaces A: Physicochemical and Engineering Aspects*, *107*, 1–56. https://doi.org/10.1016/0927-7757(95)03384-X

Sen, T. K., & Khilar, K. C. (2006). Review on subsurface colloids and colloid-associated contaminant transport in saturated porous media. *Advances in Colloid and Interface Science*, *119*(2), 71–96. https://doi.org/10.1016/j.cis.2005.09.001

Sen, T. K., Mahajan, S. P., & Khilar, K. C. (2002a). Adsorption of Cu^{2+} and Ni^{2+} on iron oxide and kaolin and its importance on Ni^{2+} transport in porous media. *Colloids and Surfaces A: Physicochemical and Engineering Aspects*, *211*(1), 91–102. https://doi.org/10.1016/S0927-7757(02)00235-2

Sen, T. K., Mahajan, S. P., & Khilar, K. C. (2002b). Colloid-associated contaminant transport in porous media: 1. Experimental studies. *AICHE Journal*, *48*(10), 2366–2374. https://doi.org/10.1002/aic.690481026

Şengör, S. S., Spycher, N., Ginn, T. R., Moberly, J. G., Peyton, B., & Sani, R. K (2007). Reductive dissolution and metal transport in Lake Coeur d'Alene sediments. In T. Bullen & Y. Wang (Eds.), *Water-rock interaction* (WRI-12, Vol. 2, pp. 895–899). Taylor & Francis Group.

Şengör, S. S., Spycher, N. F., Ginn, T. R., Sani, R. K., & Peyton, B. (2007). Biogeochemical reactive–diffusive transport of heavy metals in Lake Coeur d'Alene sediments. *Applied Geochemistry*, *22*(12), 2569–2594. https://doi.org/10.1016/j.apgeochem.2007.06.011

Séquaris, J. M., Klumpp, E., & Vereecken, H. (2013). Colloidal properties and potential release of water-dispersible colloids in an agricultural soil depth profile. *Geoderma*, *193*, 94–101. https://doi.org/10.1016/j.geoderma.2012.10.014

Šimůnek, J., He, C., Pang, L., & Bradford, S. A. (2006). Colloid-facilitated solute transport in variably saturated porous media. *Vadose Zone Journal*, *5*(3), 1035–1047. https://doi.org/10.2136/vzj2005.0151

Snousy, M. G., Rashad, A. M., Ebiad, M. A. E. S., Helmy, H. M., & El Bassier, M. A. A. (2018). Lead and associated micropollutant propagations in the North Suez Gulf, Egypt. *International Journal of Environmental Research*, *12*(3), 357–371. https://doi.org/10.1007/s41742-018-0094-y

Steefel, C. I., & Maher, K. (2009). Fluid-rock interaction: A reactive transport approach. *Reviews in Mineralogy and Geochemistry*, *70*, 485–532. https://doi.org/10.2138/rmg.2009.70.11

Steefel, C. I., Mayer, K. U., Arora, B., Appelo, C. A. J., Hammond, G., Jacques, D., Kolditz, O., Lagneau, V., Lichtner, P. C., Meussen, H., Molins, S., Parkhurst, D. L., Shao, H., Simůnek, J., Van der Lee, J., Yabusaki, S. B., & Yeh, G. T. (2015). Reactive transport codes for subsurface environmental simulation. *Computational Geoscience*, *19*, 445–478. https://doi.org/10.1007/s10596-014-9443-x

Steefel, C. I., Yabusaki, S. B., & Mayer, K. U. (2015). Reactive transport benchmarks for subsurface environmental simulation. *Computational Geosciences*, *19*(3), 439–443. https://doi.org/10.1007/s10596-015-9499-2

Stumm, W. (1977). Chemical interaction in particle separation. *Environmental Science & Technology*, *11*, 1066–1070. https://doi.org/10.1021/es60135a010

Thompson, A., Chadwick, O. A., Boman, S., & Chorover, J. (2006). Colloid mobilization during soil iron redox oscillations. *Environmental Science & Technology*, *40*(18), 5743–5749. https://doi.org/10.1021/es061203b

Torkzaban, S., Bradford, S. A., Vanderzalm, J. L., Patterson, B. M., Harris, B., & Prommer, H. (2015). Colloid release and clogging in porous media: effects of solution ionic strength and flow velocity. *Journal of Contaminant Hydrology*, *181*, 161–171. https://doi.org/10.1016/j.jconhyd.2015.06.005

Tosco, T., Bosch, J., Meckenstock, R. U., & Sethi, R. (2012). Transport of ferrihydrite nanoparticles in saturated porous media: role of ionic strength and flow rate. *Environmental Science & Technology*, *46*(7), 4008–4015. https://doi.org/10.1021/es202643c

Tournassat, C., & Appelo, C. A. J. (2011). Modelling approaches for anion-exclusion in compacted Na-bentonite. *Geochimica et Cosmochimica Acta*, *75*(13), 3698–3710. https://doi.org/10.1016/j.gca.2011.04.001

Um, W., & Papelis, C. (2002). Geochemical effects on colloid-facilitated metal transport through zeolitized tuffs from the Nevada test site. *Environmental Geology*, *43*(1–2), 209–218. https://doi.org/10.1007/s00254-002-0646-4

Wang, Y., Feng, X., Villalobos, M., Tan, W., & Liu, F. (2012). Sorption behavior of heavy metals on birnessite: Relationship with its Mn average oxidation state and implications for types of sorption sites. *Chemical Geology*, *292*, 25–34. https://doi.org/10.1016/j.chemgeo.2011.11.001

Winowiecki, L. (2002). *Geochemical cycling of heavy metals in the sediment of Lake Coeur d'Alene, Idaho* [Master's thesis, University of Idaho, Moscow].

Zhuang, J., Flury, M., & Jin, Y. (2003). Colloid-facilitated Cs transport through water-saturated Hanford sediment and Ottawa sand. *Environmental Science & Technology*, *37*(21), 4905–4911. https://doi.org/10.1021/es0264504

SUPPORTING INFORMATION

Additional supporting information can be found online in the Supporting Information section at the end of this article.

How to cite this article: Şengör, S. S., & Ünlü, K. (2023). Colloidal transport of heavy metals in low-advective-velocity environmental systems: Reactive transport model on biogeochemical and hydrodynamic impacts. *Vadose Zone Journal*, *22*, e20233. https://doi.org/10.1002/vzj2.20233